

THE CHEN–YANG VOLUME CONJECTURE FOR KNOTS IN HANDLEBODIES

FATHI BEN ARIBI AND JAMES GOSSELET

ABSTRACT. In 2015, Chen and Yang proposed a volume conjecture that stated that certain Turaev–Viro invariants of an hyperbolic 3-manifold should grow exponentially with a rate equal to the hyperbolic volume.

Since then, this conjecture has been proven or numerically tested for several hyperbolic 3-manifolds, either closed or with boundary, the boundary being either a family of tori or a family of higher genus surfaces. The current paper now provides new numerical checks of this volume conjecture for 3-manifolds with one toroidal boundary component and one geodesic boundary component.

More precisely, we study a family of hyperbolic 3-manifolds M_g introduced by Frigerio. Each M_g can be seen as the complement of a knot in an handlebody of genus g .

We provide an explicit code that computes the Turaev–Viro invariants of these manifolds M_g , and we then numerically check the Chen–Yang volume conjecture for the first six members of this family.

Furthermore, we propose an extension of the volume conjecture, where the second coefficient of the asymptotic expansion only depends on the topology of the boundary of the manifold. We numerically check this property for the manifolds M_2, \dots, M_7 and we also observe that the second coefficient grows linearly in the Euler characteristic $\chi(\partial M_g)$.

CONTENTS

1. Introduction	2
2. Materials and methods	4
3. Preliminaries	4
3.1. Ideal triangulations	4
3.2. Hyperbolic volume	4
3.3. Admissible colorings	5
3.4. Turaev–Viro invariants	6
3.5. Volume conjecture	7
4. On Frigerio’s manifolds M_g	7
4.1. Frigerio’s construction	7
4.2. Ordered triangulations and comb representation	8
4.3. Hyperbolic structure	10
4.4. Admissible colorings	10
5. Annotated code	13
5.1. Computing the hyperbolic volume of M_g	14
5.2. Computing the Turaev–Viro invariants $TV_{r,s}(M_g, \mathcal{T}_g)$	15
5.3. Asymptotic behavior of $QV_{r,2}(M_2)$ and $QV_{r,2}(M_3)$	20
6. Numerical Results	22
6.1. The case of M_2	22
6.2. The case of M_3	26

2020 *Mathematics Subject Classification.* 57K16; 57K32.

Key words and phrases. Turaev–Viro invariants; volume conjectures; hyperbolic volume; triangulations of 3-manifolds.

6.3. The cases of M_4 to M_7	29
6.4. Behavior of the coefficient $b(M_g)$ relative to g	29
7. Discussion and further directions	31
Acknowledgements	33
References	33

1. INTRODUCTION

Quantum topology began in 1984 with the definition of the Jones Polynomial [9]. Since then, several new invariants of knots and 3-manifolds were defined and, inspired by quantum field theories, the *volume conjecture* of Kashaev [10] and its variants rose to be among the most studied conjectures in quantum topology. What is intriguing about these volume conjectures is that they link quantum invariants of manifolds to the hyperbolic structure of these manifolds. In [3], Chen–Yang proposed a volume conjecture using a family $\{TV_{r,2}\}_{r \in \mathbb{N}_{\geq 3}}$ of Turaev–Viro type invariants for compact 3-manifolds.

Conjecture 1.1 (Conjecture 1.1, [3], Chen–Yang). *Let M be a compact hyperbolic 3-manifold. Then for r running over all odd integers such that $r \geq 3$,*

$$\lim_{r \rightarrow \infty} \frac{2\pi}{r-2} \log(TV_{r,2}(M)) = \text{Vol}(M),$$

where $\text{Vol}(M)$ is the hyperbolic volume of M .

This conjecture has since then been proven [4, 13, 16] or numerically tested [3, 12] for several hyperbolic 3-manifolds, mostly for manifolds without boundary, but also manifolds with toroidal boundary and manifolds with totally geodesic boundary of genus $g \geq 2$. However, there is currently no test of this conjecture for an hyperbolic 3-manifold with a boundary which has both a toroidal component and a totally geodesic boundary component of genus $g \geq 2$. In this paper, we thus propose to test the Chen–Yang volume conjecture for a family of 3-manifolds $\{M_g\}_{g \in \mathbb{N}_{\geq 2}}$, each M_g being the exterior of a knot in a handlebody of genus g . These manifolds were constructed and studied by Frigerio [5].

We will actually go one step further, as we will test an extension of Conjecture 1.1 stated as follows:

Conjecture 1.2. *Let M be a compact hyperbolic 3-manifold of volume $\text{Vol}(M)$. Then for r running over all odd integers such that $r \geq 3$,*

$$TV_{r,2}(M) \underset{r \rightarrow \infty}{\sim} \omega \cdot r^b \cdot e^{\frac{\text{Vol}(M)}{2\pi}(r-2)} \cdot \left(1 + O\left(\frac{1}{r-2}\right)\right),$$

where $\omega, b \in \mathbb{R}$ are independent of r , or equivalently,

$$\frac{2\pi}{r-2} \log(TV_{r,2}(M)) \underset{r \rightarrow \infty}{\sim} \text{Vol}(M) + b \frac{2\pi \ln(r-2)}{r-2} + c \frac{1}{r-2} + O\left(\frac{1}{(r-2)^2}\right),$$

where $b \in \mathbb{R}$ and $c \in \mathbb{C}$ are independent of r .

Variants of Conjecture 1.2 have been previously stated, proven and numerically checked, notably by Chen–Yang [2, Section 6] (for some manifolds with boundary), and by Ohtsuki [13] and Gang–Romo–Yamasaki [6] (for certain closed manifolds, via the usual quadratic relation between Reshetikhin–Turaev invariants and Turaev–Viro invariants). In the present paper, we aim to numerically test Conjecture 1.2 for Frigerio’s manifolds M_g .

A yet stronger conjecture surmises that the coefficient b in Conjecture 1.2 should only depend on the topology of the boundary ∂M . We go further and conjecture that b is linear in $\chi(\partial M)$, as stated as follows:

Conjecture 1.3. *Let \mathcal{M} be the set of compact hyperbolic 3-manifolds for which Conjecture 1.2 holds. Then, for all $M \in \mathcal{M}$, the coefficient $b(M)$ in Conjecture 1.2 only depends on the topology of ∂M , as an affine function of the Euler characteristic $\chi(\partial M)$.*

Conjecture 1.3, as stated here, might be too strong to be true. Nevertheless, in this paper, it follows from numerical computations that Conjecture 1.3 appears to hold for Frigerio’s manifolds M_g .

After reviewing preliminaries about triangulations, hyperbolic volumes, colorings of triangulations and Turaev–Viro invariants in Section 3, we discuss the manifolds M_g in Section 4: in particular we describe their ideal triangulations \mathcal{T}_g , constructed by Frigerio. We observe that these ideal triangulations admit an *ordered structure*, which means we can orient all edges in a coherent way with face gluings and such that no triangle admits a cycle.

Proposition 1.4 (Proposition 4.3). *The triangulations \mathcal{T}_g of the manifolds M_g admit an ordered structure.*

This property will not be used for the rest of the paper, but may be useful in the future for studying other quantum invariants which are only defined on ordered triangulations [1, 11], in the specific cases of these manifolds M_g .

For two fixed integers $r \geq 3$ and $s \geq 1$, the Turaev–Viro invariant $TV_{r,s}(M, \mathcal{T})$ of a triangulated manifold (M, \mathcal{T}) is defined as a sum over a (usually large) set of admissible colorings of the triangulation \mathcal{T} . Hence, in order to compute the Turaev–Viro invariants $TV_{r,s}(M_g, \mathcal{T}_g)$, we first need to describe the associated set of admissible colorings $\mathcal{A}_r(M_g, \mathcal{T}_g)$. The main theorem of this paper provides a description of $\mathcal{A}_r(M_g, \mathcal{T}_g)$ that is both clearer than the original definition and easier to transform into computer code (in Section 5.2). We now phrase it without technical details:

Theorem 1.5 (Theorem 4.8). *An admissible coloring of \mathcal{T}_g has to satisfy a certain set of admissibility conditions, which are equivalent to another explicit and more convenient set of conditions.*

The proof of Theorem 1.5 is quite lengthy but can give insights on how to simplify admissibility conditions for other examples of triangulations. The new set of conditions given by Theorem 1.5 will be used later on in Section 5.2.

In Section 6, we study the specific cases of (M_g, \mathcal{T}_g) for $2 \leq g \leq 7$. We numerically compute their hyperbolic volume (thanks to results of Frigerio [5] and Ushijima [15]) and their logarithmic Turaev–Viro invariants $QV_{r,2}(M_g) := \frac{2\pi}{r-2} \log(TV_{r,2}(M_g, \mathcal{T}_g))$ for several values of r . For increasing values of r , we observe a convergence as expected in Conjecture 1.1 (for $2 \leq g \leq 7$), and then a surprising pattern break for $g \in \{2, 3\}$.

Numerical test 1.6 (Sections 6.1.4, 6.2.4 and 6.3). *Conjectures 1.1 and 1.2 appear to hold numerically for the manifolds M_2, \dots, M_7 , barring possible numerical errors for M_2 and M_3 .*

More precisely, the graph of the function $QV_{r,2}(M_2)$ (resp. $QV_{r,2}(M_3)$) shows a converging behavior up to $r = 33$ (resp. $r = 31$) and an unexpected increase after $r = 33$ (resp. $r = 31$). The graph of the function $QV_{r,2}(M_g)$ (for $4 \leq g \leq 7$) shows a converging behavior.

We offer hypotheses to explain the previous pattern breaks, and we furthermore compute an interpolating function for the data, which not only fits the pre-break values quite well, but also provides a promising candidate for the next term b in the expected asymptotic expansion of $QV_{r,2}(M_g)$ (see Conjecture 1.2).

In Section 5 we provide our entire code (written in *SageMath*), with annotations for clarity. In particular, we program functions that compute the hyperbolic volumes and Turaev–Viro invariants for the manifolds M_g , and we list several of these values in the tables of Figures 9 and 10.

Finally, we observe a linear behavior for the second coefficient b , as expected in Conjecture 1.3.

Numerical test 1.7 (Section 6.4). *Conjecture 1.3 appears to hold numerically for the manifolds M_2, \dots, M_7 .*

The results in this article follow in part from the Master’s thesis [7] of the second author.

2. MATERIALS AND METHODS

All the calculations were performed on SageMath (a free open-source mathematics software system using Python 3), on a computer equipped with a Intel® Core™ i5-8500 CPU @ 3.00GHz × 6 processor.

3. PRELIMINARIES

3.1. Ideal triangulations. In this section, we follow some conventions of [3] and [15]. A *pseudo 3-manifold* is a topological space M such that each point p of M has an (open) neighborhood U_p that is homeomorphic to a cone over a surface. A *triangulation* \mathcal{T} of a pseudo 3-manifold M consists of a disjoint union $T_1 \sqcup \dots \sqcup T_N$ of finitely many Euclidean tetrahedra and of a collection of affine homeomorphisms between pairs of faces in $T_1 \sqcup \dots \sqcup T_N$ such that the quotient space $(T_1 \sqcup \dots \sqcup T_N) / \sim$ is homeomorphic to M . For $i \in \{0, 1, 2, 3\}$, we denote \mathcal{T}^i (resp. $\mathcal{T}^{i,\sim}$) the i -skeleton of the disjoint union of tetrahedra in \mathcal{T} (resp. the i -skeleton of the quotient space homeomorphic to M). We say that an element ν of the set $\mathcal{T}^{0,\sim}$ of vertices of M is *regular* (resp. *ideal*, *hyperideal*) if its associated neighborhood U_ν is a cone over a sphere (resp. over a torus, over a surface of genus at least 2). Finally, we say that a compact 3-manifold N with boundary admits an *ideal triangulation* \mathcal{T} if no vertices in $\mathcal{T}^{0,\sim}$ are regular, and N is obtained from the quotient space of \mathcal{T} by removing open neighborhoods U_ν of all vertices ν in $\mathcal{T}^{0,\sim}$.

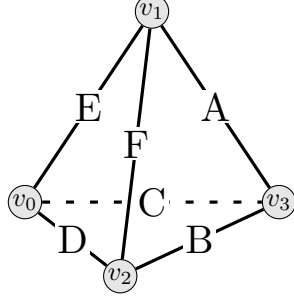
3.2. Hyperbolic volume. In [15], Ushijima gives a volume formula for a generalized hyperbolic tetrahedron with a given angle structure. Let us detail this formula and its components. Let $T = T(A, B, C, D, E, F)$ be a generalized tetrahedron in the hyperbolic space \mathbb{H}^3 whose angle structure is as in Figure 1 ($A, \dots, F \in [0, \pi]$ are dihedral angles).

Let G denote the associated Gram matrix:

$$G = \begin{pmatrix} 1 & -\cos A & -\cos B & -\cos F \\ -\cos A & 1 & -\cos C & -\cos E \\ -\cos B & -\cos C & 1 & -\cos D \\ -\cos F & -\cos E & -\cos D & 1 \end{pmatrix}.$$

Let $\text{Li}_2(z)$ be the dilogarithm function defined for $z \in \mathbb{C} \setminus [1, \infty)$ in [15, Introduction] by the analytic continuation of the following integral:

$$\text{Li}_2(x) := - \int_0^x \frac{\log(1-t)}{t} dt \quad \text{for } x \in \mathbb{R}_{>0}.$$

FIGURE 1. The configuration of dihedral angles on T .

Let I be the principal square root of -1 , $a := \exp(I \cdot A)$, $b := \exp(I \cdot B)$, ..., $f := \exp(I \cdot F)$ and let $U(z, T)$ be the complex valued function defined as follows:

$$U(z, T) := \frac{1}{2}(\text{Li}_2(z) + \text{Li}_2(abdez) + \text{Li}_2(acdfz) + \text{Li}_2(bcefz) \\ - \text{Li}_2(-abcz) - \text{Li}_2(-aefz) - \text{Li}_2(-bdfz) - \text{Li}_2(-cdez)).$$

We denote by z_+ and z_- the two complex numbers defined as follows:

$$z_{\pm} := -2 \frac{\sin A \sin D + \sin B \sin E + \sin C \sin F \pm \sqrt{\det G}}{ad + be + cf + abf + ace + bcd + def + abcdef},$$

where $\sqrt{\det G} \in i\mathbb{R}_{>0}$ is the principal square root of $\det G$.

Proposition 3.1 (Ushijima, [15] Theorem 1.1). *The hyperbolic volume $\text{Vol}(T)$ of a generalized tetrahedron $T = T(A, B, C, D, E, F)$ is given as follows:*

$$\text{Vol}(T) = \frac{1}{2} \mathfrak{J}(U(z_-, T) - U(z_+, T)),$$

where \mathfrak{J} means the imaginary part.

In Section 5.1.1 we provide a code to compute the previous functions and formula.

3.3. Admissible colorings. We will mostly follow the notations, conventions and definitions of [3, Section 2]. For the remainder of this paper, let us fix a pair $(r, s) \in \mathbb{N}^2$ such that $r \geq 3$ and $s \geq 1$. We will only specify $s = 2$ when studying the Chen–Yang volume conjecture.

Notation 3.2. Let $\frac{\mathbb{N}}{2} = \{0, \frac{1}{2}, 1, \frac{3}{2}, \dots\}$ denote the set of non-negative half-integers. Let $\frac{\mathbb{N}_{\text{odd}}}{2} = \{\frac{1}{2}, \frac{3}{2}, \frac{5}{2}, \dots\}$ denote the set of non-negative half-odd-integers. Let I_r denote the subset $\{0, \frac{1}{2}, 1, \dots, \frac{r-2}{2}\}$ of $\frac{\mathbb{N}}{2}$.

As a convention, we let $\sqrt{-x} = I\sqrt{x}$ for $x \geq 0$.

Definition 3.3. A triple (i, j, k) of elements of I_r is called *admissible* if it satisfies the following conditions:

- (i) (a) $i + j \geq k$,
- (b) $j + k \geq i$,
- (c) $k + i \geq j$,
- (ii) $i + j + k \in \mathbb{N}$,
- (iii) $i + j + k \leq r - 2$.

Definition 3.4. Let M be an hyperbolic compact 3-manifold with boundary that admits an ideal triangulation \mathcal{T} . A *coloring at level r* of (M, \mathcal{T}) is an application $c : \mathcal{T}^{1, \sim} \rightarrow I_r$. The coloring is called *admissible* if for every $T \in \mathcal{T}^3$, the triples $(c([e_{01}]), c([e_{02}]), c([e_{03}]))$, $(c([e_{01}]), c([e_{12}]), c([e_{13}]))$, $(c([e_{02}]), c([e_{12}]), c([e_{23}]))$ and

$(c([e_{03}]), c([e_{13}]), c([e_{23}]))$ are admissible, where $[e_{kl}] \in \mathcal{T}^{1,\sim}$ denotes the equivalence class under \sim of the edge e_{kl} of T (for $k, l \in \{0, 1, 2, 3\}$ such that $k \neq l$).

3.4. Turaev–Viro invariants. Recall that $r, s \in \mathbb{N}$ are such that $r \geq 3$ and $s \geq 1$.

For $n \in \mathbb{N}$, the *quantum number* $[n]$ is the real number defined by

$$[n] := \frac{\sin\left(\frac{ns\pi}{r}\right)}{\sin\left(\frac{s\pi}{r}\right)} \in \mathbb{R}.$$

For $n \in \mathbb{N}$, the *quantum factorial* $[n]!$ is defined by

$$[n]! := [n][n-1]\dots[2][1] \in \mathbb{R},$$

and, as a convention, $[0]! = 1$. For an admissible triple $(i, j, k) \in (I_r)^3$, we define

$$\Delta(i, j, k) := \sqrt{\frac{[i+j-k]![i-j+k]![-i+j+k]!}{[i+j+k+1]!}}.$$

Definition 3.5 (Quantum $6j$ -symbols). Let (i, j, k, l, m, n) be a 6-tuple of elements of I_r such that (i, j, k) , (j, l, n) , (i, m, n) and (k, l, m) are admissible.

Let $T_1 = i+j+k$, $T_2 = j+l+n$, $T_3 = i+m+n$, $T_4 = k+l+m$, $Q_1 = i+j+l+m$, $Q_2 = i+k+l+n$ and $Q_3 = j+k+m+n$.

Then the *quantum $6j$ -symbol* for the 6-tuple (i, j, k, l, m, n) is defined by

$$\begin{aligned} \left| \begin{array}{ccc} i & j & k \\ l & m & n \end{array} \right| &:= \sqrt{-1}^{-2(i+j+k+l+m+n)} \Delta(i, j, k) \Delta(j, l, n) \Delta(i, m, n) \Delta(k, l, m) \\ &\cdot \sum_{z=\max\{T_1, T_2, T_3, T_4\}}^{\min\{Q_1, Q_2, Q_3\}} \frac{(-1)^z [z+1]!}{[z-T_1]![z-T_2]![z-T_3]![z-T_4]![Q_1-z]![Q_2-z]![Q_3-z]!}. \end{aligned}$$

Proposition 3.6 (Allowed symbol permutations). Let (i, j, k, l, m, n) be a 6-tuple of elements of I_r such that (i, j, k) , (j, l, n) , (i, m, n) , (k, l, m) are admissible.

Then, we have the following allowed permutations:

$$\left| \begin{array}{ccc} i & j & k \\ l & m & n \end{array} \right| = \left| \begin{array}{ccc} j & i & k \\ m & l & n \end{array} \right| = \left| \begin{array}{ccc} i & k & j \\ l & n & m \end{array} \right| = \left| \begin{array}{ccc} i & m & n \\ l & j & k \end{array} \right| = \left| \begin{array}{ccc} l & m & k \\ i & j & n \end{array} \right| = \left| \begin{array}{ccc} l & j & n \\ i & m & k \end{array} \right|.$$

Let M be a pseudo-3-manifold that admits a triangulation \mathcal{T} . Let $R \subset \mathcal{T}^{0,\sim}$ denote the set of regular vertices. We define the *regular vertices term* as $N := \left(\sum_{i \in I_r} w_i^2\right)^{-|R|}$. Let $c : \mathcal{T}^{1,\sim} \rightarrow I_r$ be an admissible coloring at level r of (M, \mathcal{T}) . For $\eta \in \mathcal{T}^{1,\sim}$, we define the *edge term* $|\eta|_c := w_{c(\eta)}$, where $w_i := (-1)^{2i} [2i+1]$ for $i \in I_r$. For $T \in \mathcal{T}^3$, we define the *tetrahedron term* as

$$|T|_c = \begin{vmatrix} c([e_{01}]) & c([e_{02}]) & c([e_{12}]) \\ c([e_{23}]) & c([e_{13}]) & c([e_{03}]) \end{vmatrix},$$

where $[e_{kl}] \in \mathcal{T}^{1,\sim}$ denotes the equivalence class under \sim of the edge e_{kl} of T (for $k, l \in \{0, 1, 2, 3\}$ such that $k \neq l$).

Definition 3.7 (Turaev–Viro invariant). Let $m = |\mathcal{T}^{1,\sim}|$. Let $\mathcal{A}_r(M, \mathcal{T}) :=$

$$\{(c(\eta_0), \dots, c(\eta_m)) \mid c : \mathcal{T}^{1,\sim} \rightarrow I_r \text{ is an admissible coloring at level } r \text{ of } (M, \mathcal{T})\}.$$

We define the *Turaev–Viro invariant* of M as

$$TV_{r,s}(M, \mathcal{T}) := N \sum_{(c(\eta_0), \dots, c(\eta_m)) \in \mathcal{A}_r(M, \mathcal{T})} \prod_{i=0}^m |\eta_i|_c \prod_{T \in X^3} |T|_c.$$

In [3, Theorem 2.6], Chen and Yang prove that the previously defined Turaev–Viro invariant of M does not depend on the triangulation \mathcal{T} .

3.5. Volume conjecture. We can now state the Chen–Yang volume conjecture:

Conjecture 3.8 ([3], Conjecture 1.1). *Let M be a compact hyperbolic 3-manifold. Then for r running over all odd integers such that $r \geq 3$,*

$$\lim_{r \rightarrow \infty} QV_{r,2}(M) = \lim_{r \rightarrow \infty} \frac{2\pi}{r-2} \log(TV_{r,2}(M)) = \text{Vol}(M),$$

where $QV_{r,2}(M) := \frac{2\pi}{r-2} \log(TV_{r,2}(M))$ and $\text{Vol}(M)$ is the hyperbolic volume of M .

Remark 3.9. In [2, Section 6.1], Chen and Yang discuss the potential asymptotic behavior of $QV_{r,2}(M)$ in more detail than in Conjecture 3.8. In particular, observations for specific M with one boundary component lead them to ask if

$$QV_{r,2}(M) = \text{Vol}(M) + b \frac{\ln(r-2)}{r-2} + c \frac{1}{r-2} + O\left(\frac{1}{(r-2)^2}\right),$$

where the numbers b, c would depend only on M . In the examples they study, they find b to be close to π when M has one toroidal boundary component and -3π when M has one geodesic boundary component of genus 2. We rephrased this general question as Conjecture 1.2.

We will study in Sections 6.1.4 and 5.3 how likely these asymptotic behaviors seem for the manifolds M_2, M_3, \dots, M_7 (which have two boundary components each, of different genera).

4. ON FRIGERIO'S MANIFOLDS M_g

4.1. Frigerio's construction. This section follows closely the construction in [5]. Let $g \in \mathbb{N}_{\geq 2}$. Let S^3 be the one point compactification of \mathbb{R}^3 .

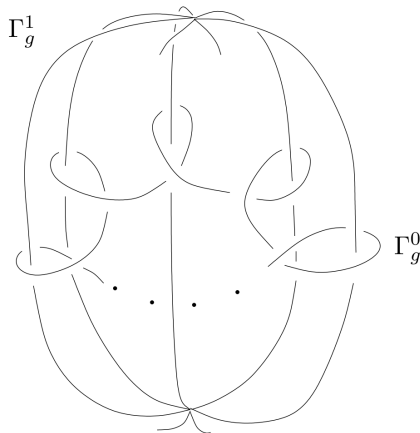


FIGURE 2. Γ_g has two components: Γ_g^0 is a knot and Γ_g^1 is a graph with $g+1$ edges and two vertices. Source: [5, Figure 1]

Let $\Gamma_g \subset S^3$ be the graph shown in Figure 2 (see Figure 3 for the cases $g = 2$ and $g = 3$). Let us denote by Γ_g^0 and Γ_g^1 the two connected components of Γ_g , where Γ_g^0 is a knot and Γ_g^1 has two vertices and $g+1$ edges. Let $U(\Gamma_g^0)$ and $U(\Gamma_g^1)$ denote open regular neighbourhoods of Γ_g^0 and Γ_g^1 . Then M_g is defined as the compact 3-manifold $M_g := S^3 \setminus \{U(\Gamma_g^0), U(\Gamma_g^1)\}$ with boundary $\partial M = (\partial M)_0 \cup (\partial M)_1$ such that $(\partial M)_0 = \partial U(\Gamma_g^0) \cong S^1 \times S^1$ and $(\partial M)_1 = \partial U(\Gamma_g^1) \cong \Sigma_g$ a genus g surface.

Remark 4.1. The 3-manifold M_g is the exterior of a knot in the handlebody of genus g as seen in Figure 4.

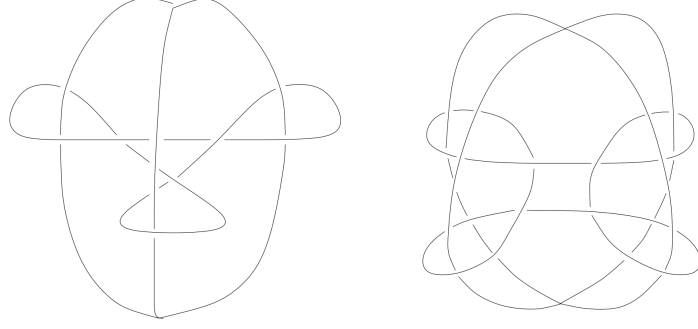


FIGURE 3. The graphs Γ_2 (on the left) and Γ_3 (on the right). Source: [5, Figure 2]

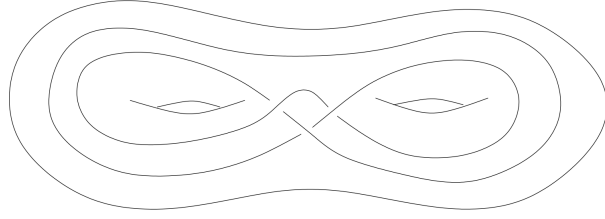


FIGURE 4. The 3-manifold M_2 as a knot complement in the handlebody of genus 2. Source: [5, Figure 3]

In [5, Section 2], Frigerio constructs an ideal triangulation of M_g . This construction is illustrated for the cases $g = 2$ and $g = 3$ in Figure 5. Let P_g be the double cone with apices ap_1 and ap_2 and based on the regular $(2g + 2)$ -gon whose vertices are $p_0, p_1, \dots, p_{2g+1}$. Let \hat{P}_g be P_g with its vertices removed. Let Y_g be the topological space obtained by gluing the faces of \hat{P}_g according to the following rules:

- For any $i = 0, 2, \dots, 2g$, the face $[ap_1, p_i, p_{i+1}]$ is identified with the face $[p_{i+1}, p_{i+2}, v_2]$ (with v_1 identified with p_{i+1} , p_i identified with p_{i+2} and p_{i+1} identified with ap_2),
- For any $i = 1, 3, \dots, 2g + 1$, the face $[ap_1, p_i, p_{i+1}]$ is identified with the face $[p_{i+2}, v_2, p_{i+1}]$ (with ap_1 identified with p_{i+2} , p_i identified with ap_2 and p_{i+1} identified with p_{i+1}).

Proposition 4.2 (Proposition 2.1, [5]). *For any $g \geq 2$, Y_g is homeomorphic to the interior of M_g .*

We can then subdivide P_g into $2g + 2$ tetrahedra by adding the vertical edge between the two apices ap_1 and ap_2 (in red in Figure 5). Such tetrahedra give an ideal triangulation of M_g .

4.2. Ordered triangulations and comb representation. We refer to [1, 11] for the following definitions. A triangulation is called *ordered* when it is endowed with an order on each quadruplet of vertices of each tetrahedron, such that the face gluings respect the vertex order. An equivalent property is that we can orient the edges of the triangulation in a compatible way with the face gluings and such that there are no cycles of length 3.

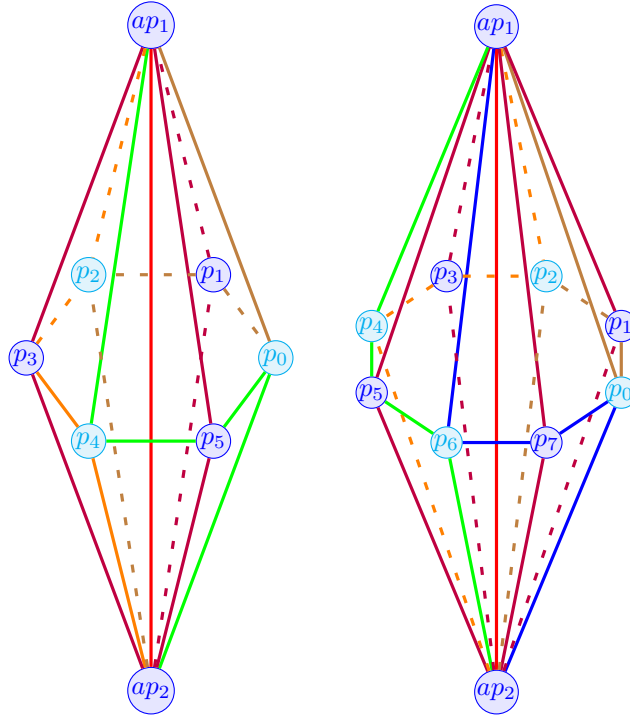


FIGURE 5. Representation of Y_2 (left) and Y_3 (right) with the red vertical edge between the two apices and identified edges and vertices have the same color.

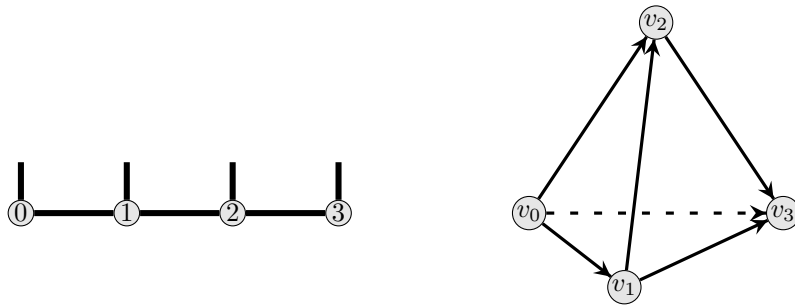


FIGURE 6. An ordered tetrahedron T (right) and its associated comb $C(T)$ (left).

A *comb* C is a line together with four spikes pointing in the same direction. The spikes are numbered 0, 1, 2 and 3 going from left to right, with the spikes pointing upward. The *comb representation* of an ordered triangulation consists in associating a comb $C(T)$ to each tetrahedron T of the triangulation, as in Figure 6; each spike numbered i corresponds to a face f^i opposed to a vertex v_i for $i \in \{0, 1, 2, 3\}$, and we join by a line the spike i of $C(T)$ to the spike j of $C(T')$ if the i -th face of T is glued to the j -th face of T' .

The comb representation provides a compact way of representing an ordered triangulation, while containing all the information of this triangulation. Moreover, comb representations are convenient for studying certain quantum invariants of ordered triangulations (such as the Teichmüller TQFT [1]). In this sense, it is

interesting to observe when a given triangulation admits an ordered structure. This is the case for Firgerio's triangulations \mathcal{T}_g , as we now state:

Proposition 4.3. *The triangulations \mathcal{T}_g of the manifolds M_g admit an ordered structure.*

The proof is quite standard, in that we exhibit a specific ordered structure (more details are in [7]). For brevity we will only refer to the examples of $g = 2$ and $g = 3$ represented in Figures 12 and 15. The associated comb representation for $g = 2$ is drawn on Figure 7.

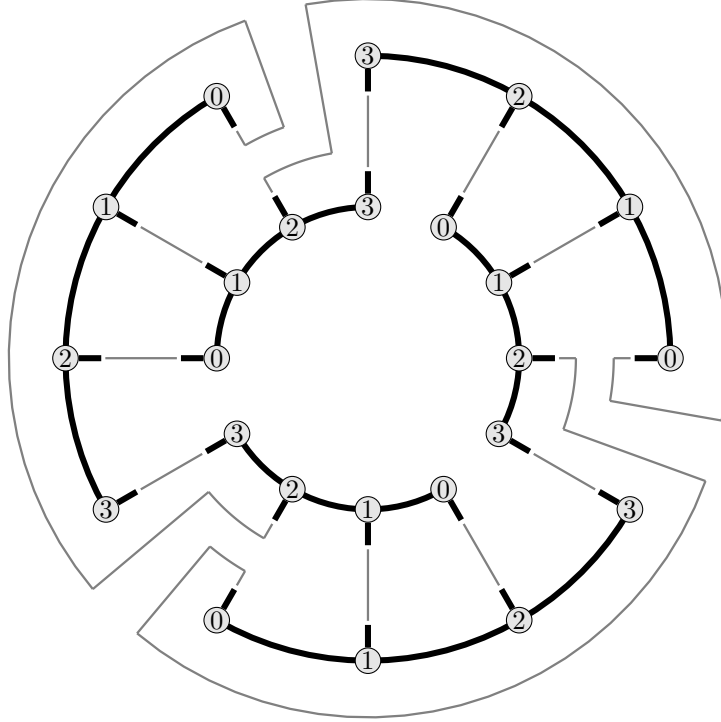


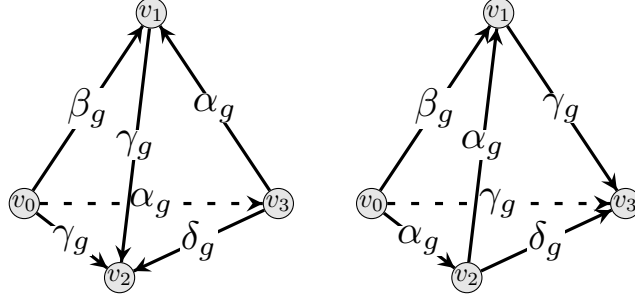
FIGURE 7. Comb representation of \mathcal{T}_2 .

4.3. Hyperbolic structure. In [5, Section 2], Frigerio provides the unique angle structure on the tetrahedra of the ideal triangulation \mathcal{T}_g that corresponds to the unique complete hyperbolic structure on the manifold M_g . Setting $\alpha_g = \frac{\pi}{2g+2}$, $\beta_g = 2\alpha_g$, $\gamma_g = \arccos((2 \cos \alpha_g)^{-1})$ and $\delta_g = \pi - 2\gamma_g$, the complete angle structure on \mathcal{T}_g follows the pattern of Figure 8: half of the $2g + 2$ tetrahedra are as the one on the left, and the other half are as the one on the right.

Both tetrahedra of Figure 8 have the same volume, and the volume of M_g is exactly $2g + 2$ times higher. Values of these volumes are computed with SageMath (see Section 5.1.2) and listed in Figure 9.

4.4. Admissible colorings. In this section we study the set of admissible colorings for the triangulations \mathcal{T}_g . The following three lemmas follow from standard arguments, are not restricted to the manifolds M_g , and will be used in the proof of Theorem 4.8. See [7] for details.

Lemma 4.4. *Let $i, k \in I_r$. Then (i, i, k) is admissible if and only if $k \in \mathbb{N}$ and $\frac{k}{2} \leq i \leq \frac{r-2-k}{2}$.*

FIGURE 8. Frigerio's angle structure on \mathcal{T}_g

Lemma 4.5. *Let $i, j, k, l, m \in I_r$ such that (i, j, k) and (k, l, m) are admissible, then $i + j + l + m \in \mathbb{N}$.*

Lemma 4.6. *Let $i, j, k \in I_r$ such that $k \in \mathbb{N}$. Then the following conditions are equivalent:*

- (i) $i + j + k \in \mathbb{N}$,
- (ii) $i + j \in \mathbb{N}$,
- (iii) either $i, j \in \mathbb{N}$ or $i, j \in \frac{\mathbb{N}_{\text{odd}}}{2}$.

Remark 4.7. Lemma 4.6 can be applied to condition (ii) of Definition 3.3 when i, j or k is in \mathbb{N} .

Let $g \in \mathbb{N}_{\geq 2}$. For a general coloring c at level r of (M_g, \mathcal{T}_g) , we need the following triples of elements of I_r to be admissible:

$$(a, b, b), \quad (a, c_g, c_0), \quad (b, c_g, c_g), \quad (b, c_g, c_0),$$

$$\text{and for all } i \in \{0, 1, 2, \dots, g-1\}, \quad (a, c_i, c_{i+1}), \quad (b, c_i, c_i), \quad (b, c_i, c_{i+1}).$$

These admissibility conditions can be rewritten like in the next theorem.

Theorem 4.8. *Let $a, b, c_0, c_1, c_2, \dots, c_g \in I_r$.*

The conditions (A), (B), (C), (D), (E), (F) and (G) defined below are simultaneously satisfied if and only if the conditions (1), (2), (3), (4), (5) and (6) defined below are simultaneously satisfied.

The conditions (A), (B), (C), (D), (E), (F) and (G) are written:

- (A) (a, b, b) is admissible,
- (B) (a, c_g, c_0) is admissible,
- (C) (b, c_g, c_g) is admissible,
- (D) (b, c_g, c_0) is admissible,
- (E) $\forall i \in \{0, 1, 2, \dots, g-1\}$, (a, c_i, c_{i+1}) is admissible,
- (F) $\forall i \in \{0, 1, 2, \dots, g-1\}$, (b, c_i, c_i) is admissible,
- (G) $\forall i \in \{0, 1, 2, \dots, g-1\}$, (b, c_i, c_{i+1}) is admissible,

The conditions (1), (2), (3), (4), (5) and (6) are written:

- (1) $a \in \mathbb{N}$,
- (2) $b \in \mathbb{N}$,
- (3) either $\forall i \in \{0, 1, 2, \dots, g\}$, $c_i \in \mathbb{N}$ or $\forall i \in \{0, 1, 2, \dots, g\}$, $c_i \in \frac{\mathbb{N}_{\text{odd}}}{2}$,
- (4) $\frac{a}{2} \leq b \leq \frac{r-2-a}{2}$,
- (5) (a) $\forall i \in \{0, 1, 2, \dots, g-1\}$, $\frac{b}{2} \leq c_{i+1} \leq \frac{r-2-b}{2}$,
- (b) $\forall i \in \{0, 1, 2, \dots, g-1\}$, $a - c_i \leq c_{i+1} \leq r - 2 - a - c_i$,
- (c) $\forall i \in \{0, 1, 2, \dots, g-1\}$, $c_i - a \leq c_{i+1} \leq a + c_i$,
- (d) $\forall i \in \{0, 1, 2, \dots, g-1\}$, $c_i - b \leq c_{i+1} \leq b + c_i$,
- (6) (a) $\frac{b}{2} \leq c_0 \leq \frac{r-2-b}{2}$,
- (b) $a - c_g \leq c_0 \leq r - 2 - a - c_g$,

- (c) $c_g - a \leq c_0 \leq a + c_g$,
(d) $c_g - b \leq c_0 \leq b + c_g$.

Proof. Let $a, b, c_0, c_1, c_2, \dots, c_g \in I_r$.

Step 1 : $(A) \iff (1) \wedge (4)$;

This step follows immediately from Lemma 4.4.

Step 2 : $(A) \wedge (E) \iff (1) \wedge (3) \wedge (4) \wedge (5b) \wedge (5c)$;

By Definition 3.3, Condition (E) is equivalent to the following conditions :

- (Ei) (a) $\forall i \in \{0, 1, 2, \dots, g-1\}, c_i + c_{i+1} \geq a$,
(b) $\forall i \in \{0, 1, 2, \dots, g-1\}, c_i + a \geq c_{i+1}$,
(c) $\forall i \in \{0, 1, 2, \dots, g-1\}, a + c_{i+1} \geq c_i$,
(Eii) $\forall i \in \{0, 1, 2, \dots, g-1\}, c_i + c_{i+1} + a \in \mathbb{N}$,
(Eiii) $\forall i \in \{0, 1, 2, \dots, g-1\}, c_i + c_{i+1} + a \leq r-2$.

To prove Step 2, we first remark that:

$$(Eia) \wedge (Eiii) \iff (5b),$$

$$(Eib) \wedge (Eic) \iff (5c).$$

It remains to prove that :

$$(A) \wedge (Eii) \iff (1) \wedge (3) \wedge (4).$$

It follows from Step 1 that :

$$(A) \wedge (Eii) \iff (1) \wedge (4) \wedge (Eii).$$

From Lemma 4.6, it follows that

$$(1) \wedge (4) \wedge (Eii) \iff (1) \wedge (4) \wedge \left(\forall i \in \{0, 1, 2, \dots, g-1\}, (c_i, c_{i+1} \in \mathbb{N}) \vee \left(c_i, c_{i+1} \in \frac{\mathbb{N}_{\text{odd}}}{2} \right) \right).$$

Finally, it follows by a quick induction that:

$$(1) \wedge (4) \wedge \left(\forall i \in \{0, 1, 2, \dots, g-1\}, (c_i, c_{i+1} \in \mathbb{N}) \vee \left(c_i, c_{i+1} \in \frac{\mathbb{N}_{\text{odd}}}{2} \right) \right) \iff (1) \wedge (4) \wedge (3).$$

Step 3 : $(A) \wedge (B) \wedge (E) \iff (1) \wedge (3) \wedge (4) \wedge (5b) \wedge (5c) \wedge (6b) \wedge (6c)$;

From Step 2, it follows that:

$$(A) \wedge (E) \iff (1) \wedge (3) \wedge (4) \wedge (5b) \wedge (5c).$$

By Definition 3.3, Condition (B) is equivalent to the following conditions :

- (Bi) (a) $c_g + c_0 \geq a$,
(b) $c_g + a \geq c_0$,
(c) $a + c_0 \geq c_g$,
(Bii) $c_g + c_0 + a \in \mathbb{N}$,
(Biii) $c_g + c_0 + a \leq r-2$.

To prove Step 3, we first remark that:

$$(Bia) \wedge (Biii) \iff (6b),$$

$$(Bib) \wedge (Bic) \iff (6c).$$

Finally, let us prove the following implication which will imply Step 3:

$$(A) \wedge (E) \implies (Bii).$$

From Step 2, it follows that

$$(A) \wedge (E) \implies (1) \wedge (3).$$

Furthermore, using Lemma 4.6, we have that:

$$(1) \wedge (3) \implies (Bii).$$

Step 4 : $(C) \wedge (F) \iff (2) \wedge (5a) \wedge (6a)$;

This step follows immediately from Lemma 4.4.

$$\text{Step 5 : } \frac{(A) \wedge (B) \wedge (C) \wedge (E) \wedge (F) \wedge (G) \iff (1) \wedge (2) \wedge (3) \wedge (4) \wedge (5a) \wedge (5b) \wedge (5c) \wedge (5d) \wedge (6a) \wedge (6b) \wedge (6c);}{\text{From Step 3, it follows that:}}$$

$$(A) \wedge (B) \wedge (E) \iff (1) \wedge (3) \wedge (4) \wedge (5b) \wedge (5c) \wedge (6b) \wedge (6c).$$

From Step 4, it follows that:

$$(C) \wedge (F) \iff (2) \wedge (5a) \wedge (6a).$$

By Definition 3.3, Condition (G) is equivalent to the following conditions :

- (Gi) (a) $\forall i \in \{0, 1, 2, \dots, g-1\}, c_i + c_{i+1} \geq b,$
- (b) $\forall i \in \{0, 1, 2, \dots, g-1\}, c_i + b \geq c_{i+1},$
- (c) $\forall i \in \{0, 1, 2, \dots, g-1\}, b + c_{i+1} \geq c_i,$
- (Gii) $\forall i \in \{0, 1, 2, \dots, g-1\}, c_i + c_{i+1} + b \in \mathbb{N},$
- (Giii) $\forall i \in \{0, 1, 2, \dots, g-1\}, c_i + c_{i+1} + b \leq r-2.$

Following what precedes, in order to prove Step 5, we only need to prove that:

$$\text{Step 5.1 } (C) \wedge (F) \implies (Gia) \wedge (Giii),$$

$$\text{Step 5.2 } (Gib) \wedge (Gic) \iff (5d),$$

$$\text{Step 5.3 } (A) \wedge (E) \implies (Gii).$$

Let us prove Step 5.1. From Step 4, it follows that

$$(C) \wedge (F) \implies (5a) \wedge (6a).$$

Furthermore, we have by adding inequalities that :

$$(5a) \wedge (6a) \implies (Gia) \wedge (Giii).$$

Step 5.2 follows immediately from the definitions.

Finally, let us prove Step 5.3. From Step 2, it follows that

$$(A) \wedge (E) \implies (1) \wedge (3).$$

Furthermore, using Lemma 4.6, we have that:

$$(1) \wedge (3) \implies (Gii).$$

This concludes the proof of Step 5.

$$\text{Step 6 : } \frac{(A) \wedge (B) \wedge (C) \wedge (D) \wedge (E) \wedge (F) \wedge (G) \iff (1) \wedge (2) \wedge (3) \wedge (4) \wedge (5a) \wedge (5b) \wedge (5c) \wedge (5d) \wedge (6a) \wedge (6b) \wedge (6c) \wedge (6d);}{\text{We prove Step 6 almost exactly as we proved Step 5. The only difference being the (G) conditions become (D) conditions and (5d) becomes (6d).}}$$

We prove Step 6 almost exactly as we proved Step 5. The only difference being the (G) conditions become (D) conditions and (5d) becomes (6d).

This concludes the proof of the theorem. \square

As we will see, Theorem 4.8 can be used to simplify the formula and computation of the Turaev–Viro invariants for the manifolds M_g , and to write a code for computing these invariants numerically (see Section 5.2).

5. ANNOTATED CODE

The following codes have been written with SageMath, a free open-source mathematics software system using Python 3. In this section, let us fix a pair $(r, s) \in \mathbb{N}^2$ such that $r \geq 3$ and $s \geq 1$. Let $g \in \mathbb{N}_{\geq 2}$. Let us recall the following notation:

Notation 5.1. Let $\frac{\mathbb{N}}{2} = \{0, \frac{1}{2}, 1, \dots\}$ denote the set of non-negative half integers. Let $\frac{\mathbb{N}_{\text{odd}}}{2} = \{\frac{1}{2}, \frac{3}{2}, \dots\}$ denote the set of non-negative half-odd-integers. Let I_r denote the subset $\{0, \frac{1}{2}, 1, \dots, \frac{r-2}{2}\}$ of $\frac{\mathbb{N}}{2}$.

5.1. Computing the hyperbolic volume of M_g . In this section, we construct a function which computes the volume of a tetrahedron from its dihedral angles, via Ushijima's volume formula (see Proposition 3.1). We then apply this function to the manifolds M_g with triangulations \mathcal{T}_g .

5.1.1. The volume formula for hyperbolic tetrahedra. We follow the steps and notation of Section 3.2. We first import the *NumPy* package which is an easy to use, open source package in Python. This package contains the function `pi` giving an approximate value of π that we will use later on. Functions imported from this package will be written in the code with the prefix `np.`, which means we access the function inside the package *NumPy*. The function `Gramdet(A,B,C,D,E,F)` computes the determinant of the Gram matrix associated to $A, B, C, D, E, F \in [0, \pi]$.

```

1 import numpy as np
2
3 def Gramdet(A,B,C,D,E,F):
4 G = matrix([[1,-cos(A),-cos(B),-cos(F)],
5 [-cos(A),1,-cos(C),-cos(E)],
6 [-cos(B),-cos(C),1,-cos(D)],
7 [-cos(F),-cos(E),-cos(D),1]])
8 res = G.determinant()
9 return res

```

LISTING 1. The determinant of the Gram matrix of T

The `U(z,A,B,C,D,E,F)` function computes $U(z, T)$ for a given complex number z and the dihedral angles A, B, C, D, E and F of a given generalized tetrahedron T . We use the `dilog(z)` function for z a complex number to compute $\text{Li}_2(z)$.

```

1 def U(z,A,B,C,D,E,F):
2 a = exp(I*A)
3 b = exp(I*B)
4 c = exp(I*C)
5 d = exp(I*D)
6 e = exp(I*E)
7 f = exp(I*F)
8
9 z1 = a*b*d*e*z
10 z2 = a*c*d*f*z
11 z3 = b*c*e*f*z
12 z4 = -a*b*c*z
13 z5 = -a*e*f*z
14 z6 = -b*d*f*z
15 z7 = -c*d*e*z
16
17 res = 1/2*(dilog(z)+dilog(z1)+dilog(z2)+dilog(z3)-dilog(z4)-dilog(z5)-
18 dilog(z6)-dilog(z7))
19 return res

```

LISTING 2. The complex valued function $U(z, T)$

Finally, the `TetVolum(A,B,C,D,E,F)` function uses the formula of Proposition 3.1 to compute the hyperbolic volume of a tetrahedron given its dihedral angles A, B, C, D, E and F .

```

1 def TetVolum(A,B,C,D,E,F):
2 a = exp(I*A)
3 b = exp(I*B)
4 c = exp(I*C)
5 d = exp(I*D)
6 e = exp(I*E)

```

```

7 f = exp(I*F)
8
9 det = Gramdet(A,B,C,D,E,F)
10
11 zminus = -2*((sin(A)*sin(D)+sin(B)*sin(E)+sin(C)*sin(F)-sqrt(det))/(a*
12         d+b*e+c*f+a*b*f+a*c*e+b*c*d+d*e*f+a*b*c*d*e*f))
13
14 zplus = -2*((sin(A)*sin(D)+sin(B)*sin(E)+sin(C)*sin(F)+sqrt(det))/(a*d
15         +b*e+c*f+a*b*f+a*c*e+b*c*d+d*e*f+a*b*c*d*e*f))
16 res = imag((U(zminus,A,B,C,D,E,F)-U(zplus,A,B,C,D,E,F))/2)
17 return res

```

LISTING 3. The hyperbolic volume of T

5.1.2. *Applying the volume formula on tetrahedra of \mathcal{T}_g .* Following Frigerio’s computation of the complete angle structure detailed in Section 4.3, we define the function **HyperbolicVolume**(g) to compute the hyperbolic volume of M_g given $g \in \{2, 3, 4, \dots\}$. Thanks to the symmetries in the complete angle structure, this function computes the hyperbolic volume of one tetrahedron and multiplies it by $2g + 2$ (the number of tetrahedra in the triangulation). We display several values for this function for some values of g in Figure 9.

```

1 def HyperbolicVolume(g):
2     Alphag=np.pi/(2*g+2)
3     Betag=2*Alphag
4     Gammag=arccos(1/(2*cos(Alphag)))
5     Deltag=np.pi - 2*Gammag
6
7     res=(2*g+2)*TetVolum(Gammag,Deltag,Gammag,Alphag,Betag,Alphag)
8     return res

```

LISTING 4. The hyperbolic volume of M_g for a given g

g	$\text{Vol}(T_g)$	$\text{Vol}(M_g)$
2	2.007682006682397	12.046092040094381
3	2.2547631818606026	18.03810545488482
4	2.3603494908554774	23.603494908554772
5	2.415787949187158	28.989455390245897
6	2.448617485457304	34.28064479640226
7	2.469695490891516	39.51512785426426
8	2.484045062029212	44.71281111652581
9	2.494259571737797	49.88519143475594
10	2.5017908556003303	55.039398823207264
100	2.5369350366401	512.4608774013002
1000	2.5373497508910896	5079.774201283962

FIGURE 9. The hyperbolic volumes of M_g and one tetrahedron T_g of \mathcal{T}_g for various values of g .

5.2. **Computing the Turaev–Viro invariants $TV_{r,s}(M_g, \mathcal{T}_g)$.** In this section, we will construct several functions in order to compute the Turaev–Viro invariants $TV_{r,s}(M_2, \mathcal{T}_2)$ and $TV_{r,s}(M_3, \mathcal{T}_3)$ given $(r, s) \in \mathbb{N}^2$ such that $r \geq 3$ and $s \geq 1$. These functions can easily be extended to compute the other Turaev–Viro invariants $TV_{r,s}(M_g, \mathcal{T}_g)$ for $g \geq 4$ (which we will do for $4 \leq g \leq 7$).

We first import the *NumPy* package as in Section 5.1.1. We also import the *cmath* package which gives us mathematical functions for complex numbers, such as square roots for negative numbers. Functions imported from *cmath* will be written with the prefix **cm.**

```
1 import numpy as np
2 import cmath as cm
```

LISTING 5. Importing NumPy and cmath

The function **quantum_number(r,s,n)** returns the quantum number $[n]$ given r , s and $n \in \mathbb{N}$.

```
1 def quantum_number(r,s,n):
2 res=sin(s*n*(np.pi)/r)/sin(s*(np.pi)/r)
3 return res
```

LISTING 6. Quantum number

The function **quantum_factorial(r,s,n)** returns the factorial of a quantum number $[n]!$ given r , s and $n \in \mathbb{N}$.

```
1 def quantum_factorial(r,s,n):
2 if n == 0:
3 return 1
4 return prod([quantum_number(r,s,i) for i in range(1, n+1)])
```

LISTING 7. Quantum factorial

The function **q_big_delta_coeff(i,j,k,r,s)** returns the coefficients $\Delta(i, j, k)$ given r , s and (i, j, k) an admissible triple of elements of I_r . Admissibility conditions ensure that $i + j - k$, $i + k - j$, $j + k - i$ and $i + j + k + 1$ are in \mathbb{N} but since the values of i , j and k can be half integers, the values $i + k - j$, $j + k - i$ and $i + j + k + 1$ are stored as rational type variable. To ensure that the function **quantum_factorial()** works, we have to change their type from rational to integers using the *int()* function. Since **quantum_number()** and thus **quantum_factorial()** can return negative values, the term we take the square root of might thus be negative. Hence we need to use the function **cm.sqrt()**, i.e the complex square root from the *cmath* package.

```
1 def q_big_delta_coeff(i,j,k,r,s):
2 argsqrt = (quantum_factorial(r,s,int(i + j - k)) * quantum_factorial(r
, s, int(i + k - j)) * quantum_factorial(r,s,int(j + k - i))) /
quantum_factorial(r,s,int(i + j + k + 1))
3
4 res = cm.sqrt(argsqrt)
5 return res
```

LISTING 8. Δ coefficients

The function **q_symbol(i, j, k, l, m, n, r, s)** returns the quantum $6j$ -symbol $\left| \begin{smallmatrix} i & j & k \\ l & m & n \end{smallmatrix} \right|$ given r , s and (i, j, k, l, m, n) a sextuple of elements of I_r such that (i, j, k) , (j, l, n) , (i, m, n) and (k, l, m) are admissible.

```
1 def q_symbol(i, j, k, l, m, n, r, s):
2 prefac = q_big_delta_coeff(i, j, k, r, s) * q_big_delta_coeff(j, l, n,
r, s) * q_big_delta_coeff(i, m, n, r, s) * q_big_delta_coeff(k, l
, m, r, s)
3
4 zmin = max(i + j + k, j + l + n, i + m + n, k + l + m)
5 zmax = min(i + j + l + m, i + k + l + n, j + k + m + n)
6
7 sumres = 0
```



```

8 for z in range(int(zmin), int(zmax) + 1):
9 den = quantum_factorial(r,s,int(z - (i + j + k))) * quantum_factorial(
    r,s,int(z - (j + l + n))) * quantum_factorial(r,s,int(z - (i + m +
    n))) * quantum_factorial(r,s,int(z - (k + l + m))) *
    quantum_factorial(r,s,int(i + j + l + m - z)) * quantum_factorial(
    r,s,int(i + k + l + n - z)) * quantum_factorial(r,s,int(j + k + m
    + n - z))
10
11 sumres = sumres + (((-1) ** z) * quantum_factorial(r,s,int(z + 1))) /
    den
12
13 res = prefac * sumres * sqrt(-1)**(int(2*(i+j+k+l+m+n)))
14 return res

```

LISTING 9. Quantum $6j$ -symbols

The function `edge(a,r,s)` yields the term $w_a := (-1)^{2a}[2a + 1]$ for r, s and $a \in I_r$.

```

1 def edge(a,r,s) :
2 res = ((-1)**(2*a))*quantum_number(r,s,int(2*a+1))
3 return res

```

LISTING 10. Edge term

The function `term(a,b,c,g,r,s)` computes one term of the sum in the Definition 3.7 applied to (M_g, \mathcal{T}_g) given r, s as before, $g \in \{2, 3, 4, \dots\}$, $a \in I_r$, $b \in I_r$ and $c = (c_0, c_1, c_2, \dots, c_g) \in I_r^{g+1}$ satisfying the conditions in Theorem 4.8. This one term is equal to the product of $w_a w_b w_{c_0} \dots w_{c_g}$ with

$$\left| \begin{array}{ccc} a & b & b \\ c_0 & c_0 & c_g \end{array} \right| \left| \begin{array}{ccc} a & b & b \\ c_0 & c_0 & c_1 \end{array} \right| \cdots \left| \begin{array}{ccc} a & b & b \\ c_i & c_i & c_{i-1} \end{array} \right| \left| \begin{array}{ccc} a & b & b \\ c_i & c_i & c_{i+1} \end{array} \right| \cdots \left| \begin{array}{ccc} a & b & b \\ c_g & c_g & c_{g-1} \end{array} \right| \left| \begin{array}{ccc} a & b & b \\ c_g & c_g & c_0 \end{array} \right|.$$

```

1 def term(a,b,c,g,r,s):
2 res=edge(a, r, s)*edge(b, r, s)
3
4 for i in range(g+1):
5 if i==0:
6 res = res * edge(c[i], r, s) * q_symbol(a, b, b, c[i], c[i], c[g], r,
    s) * q_symbol(a, b, b, c[i], c[i], c[i+1], r, s)
7 elif i==g:
8 res = res * edge(c[i], r, s) * q_symbol(a, b, b, c[i], c[i], c[i-1], r,
    s) * q_symbol(a, b, b, c[i], c[i], c[0], r, s)
9 else:
10 res = res * edge(c[i], r, s) * q_symbol(a, b, b, c[i], c[i], c[i-1], r,
    s) * q_symbol(a, b, b, c[i], c[i], c[i+1], r, s)
11
12 return res

```

LISTING 11. One term of the sum in $TV_{r,s}(M_g, \mathcal{T}_g)$ for a given admissible coloring

The function `turaevvirog2(r,s)` computes $TV_{r,s}(M_2, \mathcal{T}_2)$, while the function `turaevvirog3(r,s)` computes $TV_{r,s}(M_3, \mathcal{T}_3)$ given r and s . These two functions consists in listing all the admissible colorings in the sense of Theorem 4.8 and computing the associated term contributing to the sum in $TV_{r,s}(M_g, \mathcal{T}_g)$ via the `term()` function for $g \in \{2, 3\}$.

We now detail the reasoning behind the following code. Let $a, b, c_0, \dots, c_g \in I_r$.

The a loop: For the coloring to be admissible, a has to satisfy:

- (1) $a \in \mathbb{N}$.

The first loop is over the label a which covers all integers from 0 to $\frac{r-2}{2}$. We will refer to it as the a loop. The `floor()` function ensures that the loop ends at $\lfloor \frac{r-2}{2} \rfloor$.

The b loop: For a fixed and an admissible coloring, b has to satisfy:

- (2) $b \in \mathbb{N}$,
- (4) $\frac{a}{2} \leq b \leq \frac{r-2-a}{2}$.

We thus create, inside the a loop, a second loop over the label b (called the b loop), which covers all integers from $\frac{a}{2}$ to $\frac{r-2-a}{2}$. The **floor()** and **ceil()** functions ensure that the loop ends at $\lfloor \frac{r-2-a}{2} \rfloor$ and starts at $\lceil \frac{a}{2} \rceil$.

The two kinds of nested loops inside the b loop: For an admissible coloring, the labels c_i (for $i \in \{0, 1, 2, \dots, g\}$) have to satisfy:

- (3) either $(\forall i \in \{0, 1, 2, \dots, g\}, c_i \in \mathbb{N})$ or $(\forall i \in \{0, 1, 2, \dots, g\}, c_i \in \frac{\mathbb{N}_{odd}}{2})$.

We denote those two categories as *integer states* and *half-integer states*. Thus, we create two different loops inside the b loop (one for each).

The first family of nested loops, for integer states: Let us assume $(\forall i \in \{0, \dots, g\}, c_i \in \mathbb{N})$. For a fixed b and an admissible coloring, the label c_0 has to satisfy:

- (6a) $\frac{b}{2} \leq c_0 \leq \frac{r-2-b}{2}$.

We thus create, inside the b loop, a loop over the label c_0 , the c_0 loop, which covers all integers from $\lfloor \frac{b}{2} \rfloor$ to $\lfloor \frac{r-2-b}{2} \rfloor$. This c_0 loop will contain a new c_1 loop, which will in turn contain a c_2 loop, and so on until a final c_g loop. Let us now detail how this induction works. For $i \in \{0, \dots, g-1\}$, for fixed a, b, c_i and an admissible coloring, the label c_{i+1} has to satisfy the following conditions:

- (5a) $\frac{b}{2} \leq c_{i+1} \leq \frac{r-2-b}{2}$,
- (5b) $a - c_i \leq c_{i+1} \leq r - 2 - a - c_i$,
- (5c-d) $c_i - \min(a, b) \leq c_{i+1} \leq c_i + \min(a, b)$.

For all $i \in \{0, \dots, g-1\}$, we create in the loop c_i two variables m_{i+1} and M_{i+1} : m_{i+1} is the maximum of the three lower bounds on c_{i+1} and M_{i+1} is the minimum of the three upper bounds on c_{i+1} . We thus create, inside the c_i loop, a loop over the label c_{i+1} (called the c_{i+1} loop), which ranges to all integers from $\lceil m_{i+1} \rceil$ to $\lfloor M_{i+1} \rfloor$. Finally, for fixed a, b, c_0, \dots, c_g , for the coloring to be admissible, the following conditions also need to be satisfied:

- (6b) $a - c_g \leq c_0 \leq r - 2 - a - c_g$,
- (6c-d) $c_g - \min(a, b) \leq c_0 \leq c_g + \min(a, b)$.

Hence we add an **if** loop that checks those two conditions. If they are satisfied, we then compute the term associated to the coloring $(a, b, c_0, c_1, \dots, c_g)$ via **term()**.

The second family of nested loops, for half-integer states: Once we have covered all the integer states, we create inside the b loop, a second loop over the label c_0 , which covers all half-integers from $\lfloor \frac{b}{2} \rfloor + \frac{1}{2}$ to $\lfloor \frac{r-2-b}{2} \rfloor - \frac{1}{2}$. The function **np.arange()** allows us to start and end loops at non-integer values and specify the step of the loop to be 1. The rest of this new c_0 loop is constructed in the same way as for the c_0 loop for integer states, but the nested loops are over half-integers instead of integers.

Conclusion: As proved in Theorem 4.8, these loops go over all admissible states, thus we obtain a numerical value of the exact formula $TV_{r,s}(M_g, \mathcal{T}_g)$ for $g \in \{2, 3\}$. In the same way, one can construct a function which computes $TV_{r,s}(M_g, \mathcal{T}_g)$ for $g \geq 4$ (one would simply need to add more nested loops in the two families). In the current project, we did exactly this: we defined the functions **turaevvirog4(r,s)**, **turaevvirog5(r,s)**, **turaevvirog6(r,s)** and **turaevvirog7(r,s)**, but for the sake of brevity we do not write their codes here (their codes can be easily guessed from the detailed examples of **turaevvirog2(r,s)** and **turaevvirog3(r,s)**).

```

1 def turaevvirog2(r,s):
2     res= 0
3     for a in range(floor((r-2)/2)+1):

```

```

4 for b in range(ceil(a/2), floor((r-2-a)/2)+1):
5 m=min(a,b)
6 for c0 in range(ceil(b/2), floor((r-2-b)/2)+1):
7 m1=max(c0-m, a-c0, b/2)
8 M1=min(c0+m, r-2-a-c0, (r-2-b)/2)
9 for c1 in range(ceil(m1), floor(M1)+1):
10 m2=max(c1-m, a-c1, b/2)
11 M2=min(c1+m, r-2-a-c1, (r-2-b)/2)
12 for c2 in range(ceil(m2), floor(M2)+1):
13 if (-m<=c2-c0<=m) and (a<=c2+c0<=r-2-a):
14 c=[c0, c1, c2]
15 res=res+term(a,b,c,2,r,s)
16
17 for c0 in np.arange(floor(b/2)+1/2, ceil((r-2-b)/2), 1):
18 m1=max(c0-m, a-c0, b/2)
19 M1=min(c0+m, r-2-a-c0, (r-2-b)/2)
20 for c1 in np.arange(floor(m1)+1/2, ceil(M1), 1):
21 m2=max(c1-m, a-c1, b/2)
22 M2=min(c1+m, r-2-a-c1, (r-2-b)/2)
23 for c2 in np.arange(floor(m2)+1/2, ceil(M2), 1):
24 if (-m<=c2-c0<=m) and (a<=c2+c0<=r-2-a):
25 c=[c0, c1, c2]
26 res=res+term(a,b,c,2,r,s)
27 return res

```

LISTING 12. $TV_{r,s}(M_2, \mathcal{T}_2)$

```

1 def turaevvirog3(r,s):
2 res= 0
3 for a in range(floor((r-2)/2)+1):
4 for b in np.arange(ceil(a/2), floor((r-2-a)/2)+1, 1):
5 m=min(a,b)
6 for c0 in np.arange(ceil(b/2), floor((r-2-b)/2)+1, 1):
7 m1=max(c0-m, a-c0, b/2)
8 M1=min(c0+m, r-2-a-c0, (r-2-b)/2)
9 for c1 in np.arange(ceil(m1), floor(M1)+1, 1):
10 m2=max(c1-m, a-c1, b/2)
11 M2=min(c1+m, r-2-a-c1, (r-2-b)/2)
12 for c2 in np.arange(ceil(m2), floor(M2)+1, 1):
13 m3=max(c2-m, a-c2, b/2)
14 M3=min(c2+m, r-2-a-c2, (r-2-b)/2)
15 for c3 in np.arange(ceil(m3), floor(M3)+1, 1):
16 if (-m<=c3-c0<=m) and (a<=c3+c0<=r-2-a):
17 c=[c0, c1, c2, c3]
18 res=res+term(a,b,c,3,r,s)
19
20 for c0 in np.arange(floor(b/2)+1/2, ceil((r-2-b)/2), 1):
21 m1=max(c0-m, a-c0, b/2)
22 M1=min(c0+m, r-2-a-c0, (r-2-b)/2)
23 for c1 in np.arange(floor(m1)+1/2, ceil(M1), 1):
24 m2=max(c1-m, a-c1, b/2)
25 M2=min(c1+m, r-2-a-c1, (r-2-b)/2)
26 for c2 in np.arange(floor(m2)+1/2, ceil(M2), 1):
27 m3=max(c2-m, a-c2, b/2)
28 M3=min(c2+m, r-2-a-c2, (r-2-b)/2)
29 for c3 in np.arange(floor(m3)+1/2, ceil(M3), 1):
30 if (-m<=c3-c0<=m) and (a<=c3+c0<=r-2-a):
31 c=[c0, c1, c2, c3]

```

```

32 res=res+term(a,b,c,3,r,s)
33 return res

```

LISTING 13. $TV_{r,s}(M_3, \mathcal{T}_3)$

5.3. Asymptotic behavior of $QV_{r,2}(M_2)$ and $QV_{r,2}(M_3)$. The function **quantumvirog2(r,s)** computes $QV_{r,s}(M_2) = \frac{s\pi}{r-2} \log(TV_{r,s}(M_2, \mathcal{T}_2))$ given $(r, s) \in \mathbb{N}^2$ such that $r \geq 3$ and $s \geq 1$.

```

1 def quantumvirog2(r,s):
2 res=(s*(np.pi)/(r-2))*log(turaevvirog2(r,s))
3 return res

```

LISTING 14. $QV_{r,s}(M_2, \mathcal{T}_2)$

The function **quantumvirog3(r,s)** computes $QV_{r,s}(M_3) = \frac{s\pi}{r-2} \log(TV_{r,s}(M_3, \mathcal{T}_3))$ $(r, s) \in \mathbb{N}^2$ such that $r \geq 3$ and $s \geq 1$.

```

1 def quantumvirog3(r,s):
2 res=(s*(np.pi)/(r-2))*log(turaevvirog3(r,s))
3 return res

```

LISTING 15. $QV_{r,s}(M_3, \mathcal{T}_3)$

Similarly, the definitions of **quantumvirog4(r,s)**, **quantumvirog5(r,s)**, **quantumvirog6(r,s)** and **quantumvirog7(r,s)** follow immediately.

Let us recall that we aim for a numerical test of Conjecture 1.1. Thus, we set $s = 2$ in order to numerically compute $QV_{r,2}(M_2)$ and $QV_{r,2}(M_3)$.

Note that, for some r it happens that $TV_{r,2}(M_2, \mathcal{T}_2)$ is negative. Since we require the argument of the complex logarithm function to be in $[0, 2\pi[$, the imaginary part of $QV_{r,2}(M_2)$ is either 0 when $TV_{r,2}(M_2, \mathcal{T}_2)$ is positive or $\frac{2\pi^2}{r}$ when $TV_{r,2}(M_2, \mathcal{T}_2)$ is negative, which converges to 0 as $r \rightarrow \infty$. Therefore to test the convergence of $QV_{r,2}(M_2)$ we can forget about imaginary parts and consider only the real parts.

We compute the function **quantumvirog2(r,s)** for $s = 2$ and increasing values of r , and we obtain the table of values of $\Re(QV_{r,2}(M_2))$ shown in Figure 10. We use the numerical approximation **.n()** with the best available precision (around **prec = 180**).

```

1 quantumvirog2(r,2).real().n(prec=180)

```

LISTING 16. Numerical approximation of $\Re(QV_{r,2}(M_2))$

Similarly, we use the functions **quantumvirog3(r,s)**, \dots , **quantumvirog7(r,s)** for $s = 2$ and increasing values of r , and we display the values of $\Re(QV_{r,2}(M_g))$ in Figure 10.

As we will detail in Section 6, we obtain surprising values for high r and $g = 2, 3$, probably due to numerical errors. Those values are written in red in Figure 10.

In the following code, we look for the best interpolation of our data for the values $\Re(QV_{r,2}(M_2))$, when $5 \leq r \leq 33$. We look for a model of the form $a + b \frac{\ln(r-2)}{r-2} + c \frac{1}{r-2}$ (as in Conjecture 1.2). We use the function **find_fit**.

```

1 data=[(2*i+1, quantumvirog2(2*i+1,2).real().n(prec=180)) for i in range
2 (2,15)]
3 var('a, b, c, r')
4 model(r)= a+ b*2*pi*ln(r-2)/(r-2) + c/(r-2)
5
6 sol = find_fit(data,model)
7 show(sol)

```

LISTING 17. 3-term interpolation of $\Re(QV_{r,2}(M_2))$ for $5 \leq r \leq 33$.

r	$\mathcal{R}(QV_{r,2}(M_2))$	r	$\mathcal{R}(QV_{r,2}(M_3))$	r	$\mathcal{R}(QV_{r,2}(M_4))$
5	8.14385123663626	5	11.49177317419101	5	14.51784517894469
7	9.18650442759997	7	12.80934693191113	7	16.30280237431099
9	9.65004427173429	9	13.58615197340893	9	17.32714285662395
11	9.96879239401443	11	14.12955507845825	11	18.05414567452926
13	10.20513879726808	13	14.53997951590672	13	18.60945703261760
15	10.38914324592799	15	14.86388896169300	15	19.05151621992931
17	10.53704472005768	17	15.12724763049115	17	19.41350816169271
19	10.65879117905018	19	15.34618602238218	19	19.71628402919349
21	10.76091340012164	21	15.53141775410042	21	19.97380655712918
23	10.84790597624064	23	15.69039789582600	23	20.19586182173212
25	10.92297357052110	25	15.82849506550996	25	20.38962564202214
27	10.98846715752597	27	15.94972272572273	27	20.54717170623221
29	11.04614827534519	29	16.05847664488577		
31	11.09819658700029	31	16.12064941438458		
33	11.10744853337351	33	16.64108419344305		
35	10.85076510281595	35	17.23677472848113		
37	11.70823932238226	37	17.65793100469928		
39	12.05034471052339	39	18.19438875927008		
41	12.57984278565481				
43	13.01497045469742				
45	13.57883304172589				
47	13.99851452347661				

r	$\mathcal{R}(QV_{r,2}(M_5))$	r	$\mathcal{R}(QV_{r,2}(M_6))$	r	$\mathcal{R}(QV_{r,2}(M_7))$
5	17.56864290428003	5	20.59635740610918	5	23.62294303366446
7	19.74442367439225	7	23.16334886690935	7	26.57176683519978
9	20.99442151342528	9	24.62826235095652	9	28.24541308192440
11	21.88836919170208	11	25.68044858255137	11	29.45065948405797
13	22.57622952582667	13	26.49408736663125	13	30.38589828885670
15	23.12700521166837	15	27.14829604792329	15	31.14019388548824
17	23.58015181610567	17	27.68837084809290	17	31.76448809338449
19	23.96067740594393	19	28.14316996246829	19	32.29128792277911
21	24.28544874705841	21	28.53221301857429		
23	24.56622464869820	23	28.85466729936771		

FIGURE 10. Values of $\mathcal{R}(QV_{r,2}(M_g))$ for $2 \leq g \leq 7$ and $r \geq 5$ (assumed numerical errors are written in red).

We find the values

$$a = 11.86209740389381, b = -0.835561949347834, c = -5.310168450722084,$$

and in particular a constant term a equal to the expected hyperbolic volume up to

$$\frac{12.046092040094381 - 11.86209740389381}{12.046092040094381} \approx 1.5\%.$$

We then do the same for M_3 , in the following code.

```

1 data=[(2*i+1, quantumvirog3(2*i+1,2).real().n(prec=180)) for i in range
2 (2,14)]
3
4 var('a, b, c, r')
```

```

5 model(r) = a + b*2*pi*ln(r-2)/(r-2) + c/(r-2)
6
7 sol = find_fit(data, model)
8 show(sol)

```

LISTING 18. 3-term interpolation of $\mathcal{R}(QV_{r,2}(M_3))$ for $5 \leq r \leq 31$.

We find the values

$$a = 17.712568980467715, b = -1.95506206171866, c = -5.092760978446523,$$

and in particular a constant term a equal to the expected hyperbolic volume up to

$$\frac{18.03810545488482 - 17.712568980467715}{18.03810545488482} \approx 1.8\%.$$

For each $g \in \{4, \dots, 7\}$, we interpolate all available values of $\mathcal{R}(QV_{r,2}(M_g))$ with the same model (since no numerical strangeness occur in these cases). The values for a, b, c are listed in Figure 11.

g	r_{max}	$\text{Vol}(M_g)$	a	b	c	$\frac{\text{Vol}(M_g) - a}{\text{Vol}(M_g)}$
2	33	12.04609204	11.86209740	-0.83556194	-5.31016845	$\approx 1.5\%$
3	31	18.03810545	17.71256898	-1.95506206	-5.09276097	$\approx 1.8\%$
4	27	23.60349490	22.91592390	-2.65679563	-6.74587906	$\approx 2.9\%$
5	23	28.98945539	27.83557719	-3.23491649	-8.35921398	$\approx 3.9\%$
6	23	34.28064479	32.73892860	-3.85245863	-9.69525194	$\approx 4.5\%$
7	19	39.51512785	37.25645299	-4.15342419	-12.1205935	$\approx 5.7\%$

FIGURE 11. Values of the interpolating coefficients a, b, c for the model $a + b \cdot \frac{2\pi \ln(r-2)}{r-2} + c \cdot \frac{1}{r-2}$ for $\mathcal{R}(QV_{r,2}(M_g))$, with $5 \leq r \leq r_{max}$.

6. NUMERICAL RESULTS

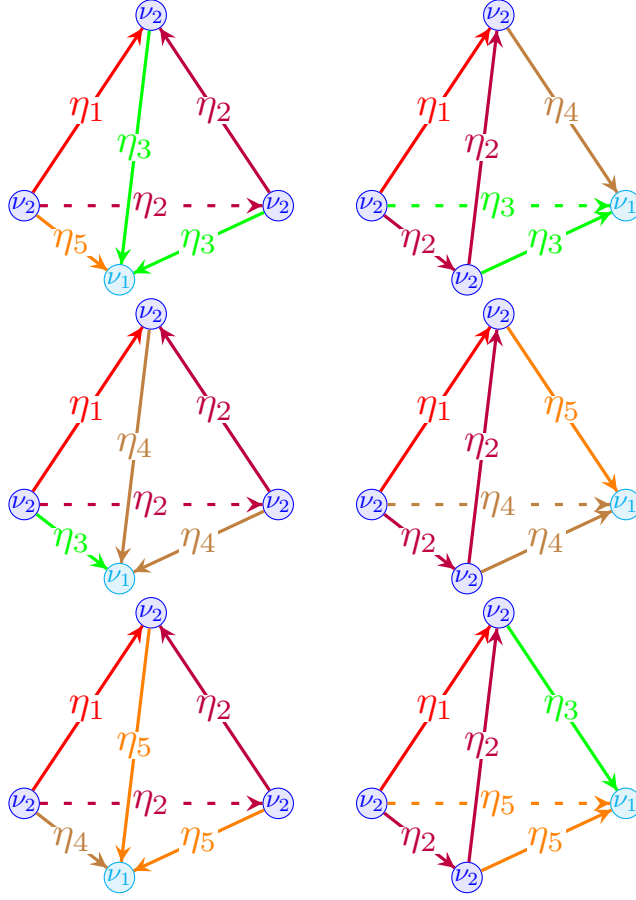
6.1. The case of M_2 . Let us now state the relevant structures and invariants of M_2 , which will then allow us to numerically check the volume conjecture for this manifold.

6.1.1. Triangulation. Figure 12 displays the ideal triangulation \mathcal{T}_g of M_g in the case $g = 2$ (note that some gluing information is not directly stated in the picture for clarity). The 0-skeleton $(\mathcal{T}_2)^{0,\sim}$ has two elements ν_1 (corresponding to the toroidal boundary component) and ν_2 (corresponding to the boundary component of genus 2). The 1-skeleton $(\mathcal{T}_2)^{1,\sim}$ contains five classes η_1, \dots, η_5 .

6.1.2. Hyperbolic structure. As a specific case of Section 4.3, the unique complete hyperbolic structure on the manifold M_2 is given by the angles

$$\alpha_2 = \frac{\pi}{6}, \quad \beta_2 = 2\alpha_2 = \frac{\pi}{3}, \quad \gamma_2 = \arccos((2 \cos \alpha_2)^{-1}), \quad \delta_2 = \pi - 2\gamma_2,$$

and the hyperbolic volume of M_2 is computed (via the code of Section 5.1.2) to be $\text{Vol}(M_2) = 12.046092040094381\dots$ (which corresponds to the value computed with *Orb* in [8]).

FIGURE 12. The ordered ideal triangulation \mathcal{T}_2 of the 3-manifold M_2

6.1.3. *Admissible colorings and Turaev–Viro Invariants.* From Definition 3.7, we compute the edge terms and tetrahedron terms contributing to $TV_{r,s}(M_2, \mathcal{T}_2)$. Since \mathcal{T}_2 has no regular vertices, the regular vertices term is thus $N = (\sum_{i \in I_r} w_i^2)^0 = 1$.

Let (a, b, c_0, c_1, c_2) be a quintuple of elements of I_r . A coloring $c : X_{\sim}^1 \rightarrow I_r$ such as in Figure 13 is admissible if and only if it satisfies the conditions of Theorem 4.8, thus

$$\mathcal{A}_r(M_2, \mathcal{T}_2) = \left\{ \begin{array}{l} \left(\begin{array}{l} a \\ b \\ c_0 \\ c_1 \\ c_2 \end{array} \right) \in I_r^5 \quad \left| \quad \begin{array}{l} a, b \in \mathbb{N}, \\ \frac{a}{2} \leq b \leq \frac{r-2-a}{2}, \\ \text{either } c_0, c_1, c_2 \in \mathbb{N} \text{ or } c_0, c_1, c_2 \in \frac{\mathbb{N}_{\text{odd}}}{2}, \\ \max\left(\frac{b}{2}, a - c_3, c_3 - \min(a, b)\right) \leq c_0, \\ c_0 \leq \min\left(\frac{r-2-b}{2}, r - 2 - a - c_3, \min(a, b) + c_3\right), \\ \max\left(\frac{b}{2}, a - c_0, c_0 - \min(a, b)\right) \leq c_1, \\ c_1 \leq \min\left(\frac{r-2-b}{2}, r - 2 - a - c_0, \min(a, b) + c_0\right), \\ \max\left(\frac{b}{2}, a - c_1, c_1 - \min(a, b)\right) \leq c_2, \\ c_2 \leq \min\left(\frac{r-2-b}{2}, r - 2 - a - c_1, \min(a, b) + c_1\right). \end{array} \right. \end{array} \right\}.$$

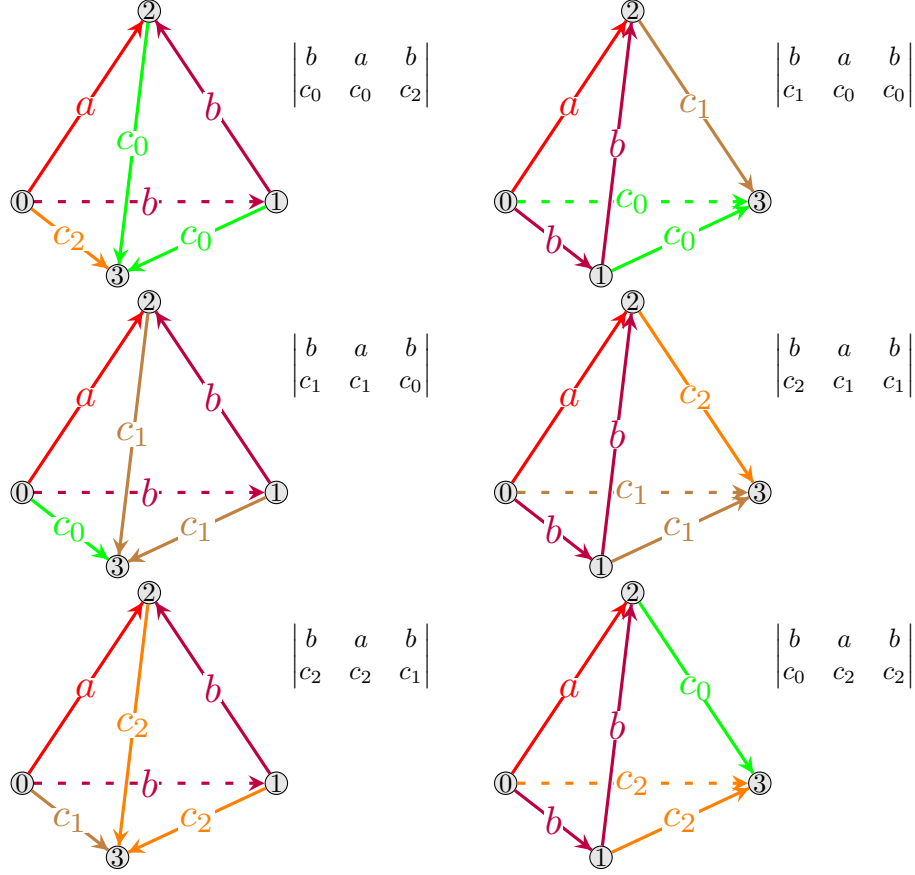


FIGURE 13. The coloring c of the ideal tetrahedra of \mathcal{T}_2 together with their respective tetrahedron terms

From Figure 13, we can determine the six tetrahedron terms $|T|_c$ and five edge terms $|\eta|_c$ associated to the coloring c which gives us the following equation:

$$TV_{r,s}(M_2, \mathcal{T}_2) = \sum_{(a,b,c_0,c_1,c_2) \in \mathcal{A}_r(M_2, \mathcal{T}_2)} w_a w_b w_{c_0} w_{c_1} w_{c_2} \cdot \begin{matrix} \begin{vmatrix} b & a & b \\ c_0 & c_0 & c_2 \end{vmatrix} \begin{vmatrix} b & a & b \\ c_1 & c_0 & c_0 \end{vmatrix} \\ \begin{vmatrix} b & a & b \\ c_1 & c_1 & c_0 \end{vmatrix} \begin{vmatrix} b & a & b \\ c_2 & c_1 & c_1 \end{vmatrix} \\ \begin{vmatrix} b & a & b \\ c_2 & c_2 & c_1 \end{vmatrix} \begin{vmatrix} b & a & b \\ c_0 & c_2 & c_2 \end{vmatrix} \end{matrix}.$$

Using Proposition 3.6 and a bit of reordering, we can rewrite the summation as:

$$TV_{r,s}(M_2, \mathcal{T}_2) = \sum_{(a,b,c_0,c_1,c_2) \in \mathcal{A}_r(M_2, \mathcal{T}_2)} w_a w_b w_{c_0} w_{c_1} w_{c_2} \cdot \begin{matrix} \begin{vmatrix} a & b & b \\ c_0 & c_0 & c_2 \end{vmatrix} \begin{vmatrix} a & b & b \\ c_0 & c_0 & c_1 \end{vmatrix} \\ \begin{vmatrix} a & b & b \\ c_1 & c_1 & c_0 \end{vmatrix} \begin{vmatrix} a & b & b \\ c_1 & c_1 & c_2 \end{vmatrix} \\ \begin{vmatrix} a & b & b \\ c_2 & c_2 & c_1 \end{vmatrix} \begin{vmatrix} a & b & b \\ c_2 & c_2 & c_0 \end{vmatrix} \end{matrix}.$$

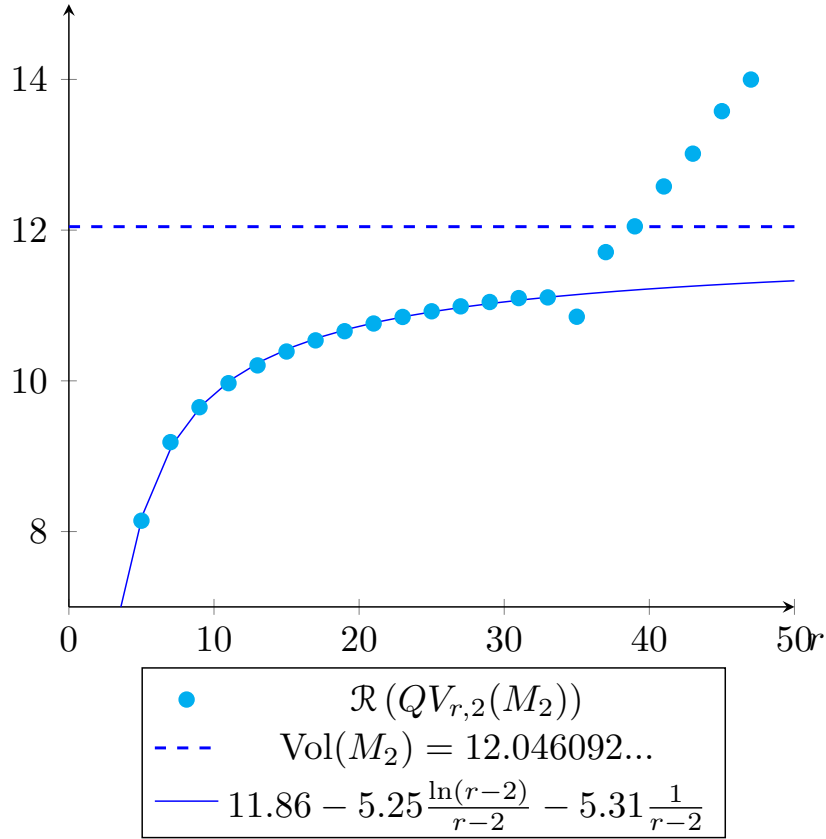


FIGURE 14. Graph of the values of $\Re(QV_{r,2}(M_2))$ (for $5 \leq r \leq 47$, blue dots) compared with the hyperbolic volume $\text{Vol}(M_2)$ (dashed and blue) and an interpolation of $\Re(QV_{r,2}(M_2))$ for $r \leq 33$ (blue curve).

6.1.4. *Numerical check of the volume conjecture.* Recall that we compute and study the behavior of $QV_{r,2}(M) := \frac{2\pi}{r-2} \log(TV_{r,2}(M))$. Figure 14 displays the values of $\Re(QV_{r,2}(M_2))$ for $5 \leq r \leq 47$ (blue dots), computed with maximal available precision via the code of Section 5.2.

For $r \leq 33$, we observe the expected convergence to the hyperbolic volume $\text{Vol}(M_2)$ (displayed with the blue dashed line); more precisely, when we fit the data for $5 \leq r \leq 33$ with the model $a + b\frac{\ln(r-2)}{r-2} + c\frac{1}{r-2}$ (see Section 5.3), we find a constant term which is very close to $\text{Vol}(M_2)$ (up to 1.5%), and the interpolating function found by SageMath (displayed in a full blue curve) appears to be close to the blue dots.

However, a strange behavior starts at $r = 35$, and the values of $\Re(QV_{r,2}(M_2))$ break the expected pattern. We offer a possible explanation that is still compatible with Conjecture 3.8: since the Turaev–Viro invariants are computed as sums of a large set of terms (exponentially many in r) which may have vastly different orders of magnitude, the numerical approximations of the computer might truncate away subtle parts of the terms in the sum, which translates to larger and larger errors in the final results.

To test this theory, we computed the same values with smaller precision, on the same machine, expecting to find different values for high r . However, it was not the case. Nevertheless, we observed that a *different computer* yielded slightly different

numerical values than the one stated in this paper, the difference increasing as r grew larger.

Such numerical errors for large r seem unavoidable when computing Turaev–Viro invariants, especially for triangulations with a large number of tetrahedra. One can for instance compare the maximum values of r that were studied for triangulations with less than 4 tetrahedra in [3], and the ones in this paper, where M_2 has 6 tetrahedra, M_3 has 8 tetrahedra, and so on.

If we restrict to the values for $r \leq 33$, Conjectures 1.1 and 1.2 seem satisfied for M_2 , as we observe the expected asymptotic behavior with small deviations.

6.2. The case of M_3 .

6.2.1. *Triangulation.* Figure 15 displays the ideal triangulation \mathcal{T}_g of M_g in the case $g = 3$. The 0-skeleton $(\mathcal{T}_3)^{0,\sim}$ has two elements ν_1 (corresponding to the toroidal boundary component) and ν_2 (corresponding to the boundary component of genus 3). The 1-skeleton $(\mathcal{T}_3)^{1,\sim}$ contains six classes η_1, \dots, η_6 .

6.2.2. *Hyperbolic structure.* As a specific case of Section 4.3, the unique complete hyperbolic structure on the manifold M_3 is given by the angles

$$\alpha_3 = \frac{\pi}{8}, \quad \beta_3 = 2\alpha_3 = \frac{\pi}{4}, \quad \gamma_3 = \arccos((2 \cos \alpha_3)^{-1}), \quad \delta_3 = \pi - 2\gamma_3,$$

and the hyperbolic volume of M_3 is computed (via the code of Section 5.1.2) to be $\text{Vol}(M_3) = 18.03810545488482\dots$

6.2.3. *Admissible colorings and Turaev–Viro Invariants.* Using Definition 3.7 for (M_3, \mathcal{T}_3) , we can determine the edge terms and tetrahedron terms contributing to $TV_{r,s}(M_3, \mathcal{T}_3)$. Since there are no regular vertices in \mathcal{T}_3 , the regular vertices term is thus $N = (\sum_{i \in I_r} w_i^2)^0 = 1$.

Let $(a, b, c_0, c_1, c_2, c_3)$ be a sextuple of elements of I_r . A coloring $c : X_r^1 \rightarrow I_r$ such as in Figure 16 is admissible if and only if it satisfies the conditions of Theorem 4.8, thus

$$\mathcal{A}_r(M_3, \mathcal{T}_3) = \left\{ \begin{pmatrix} a \\ b \\ c_0 \\ c_1 \\ c_2 \\ c_3 \end{pmatrix} \in I_r^5 \left| \begin{array}{l} a, b \in \mathbb{N}, \\ \frac{a}{2} \leq b \leq \frac{r-2-a}{2}, \\ \text{either } c_0, c_1, c_2 \in \mathbb{N} \text{ or } c_0, c_1, c_2 \in \frac{\mathbb{N}_{\text{odd}}}{2}, \\ \max\left(\frac{b}{2}, a - c_3, c_3 - \min(a, b)\right) \leq c_0, \\ c_0 \leq \min\left(\frac{r-2-b}{2}, r - 2 - a - c_3, \min(a, b) + c_3\right), \\ \max\left(\frac{b}{2}, a - c_0, c_0 - \min(a, b)\right) \leq c_1, \\ c_1 \leq \min\left(\frac{r-2-b}{2}, r - 2 - a - c_0, \min(a, b) + c_0\right), \\ \max\left(\frac{b}{2}, a - c_1, c_1 - \min(a, b)\right) \leq c_2, \\ c_2 \leq \min\left(\frac{r-2-b}{2}, r - 2 - a - c_1, \min(a, b) + c_1\right), \\ \max\left(\frac{b}{2}, a - c_2, c_2 - \min(a, b)\right) \leq c_3, \\ c_3 \leq \min\left(\frac{r-2-b}{2}, r - 2 - a - c_2, \min(a, b) + c_2\right) \end{array} \right\}.$$

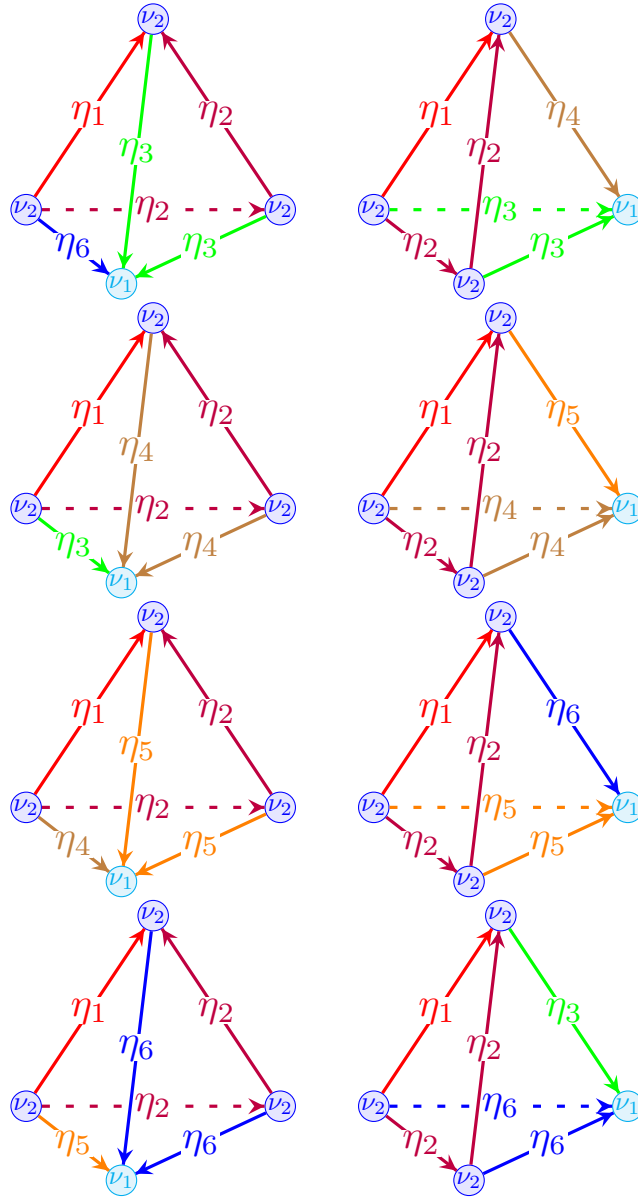


FIGURE 15. The ordered ideal triangulation \mathcal{T}_3 of the 3-manifold M_3

From Figure 16, we can determine the eight tetrahedron terms $|T|_c$ and six edge terms $|\eta|_c$ associated to the coloring c which gives us the following equation:

$$TV_{r,s}(M_3, \mathcal{T}_3) = \sum_{(a,b,c_0,c_1,c_2,c_3) \in \mathcal{A}_r(M_3, \mathcal{T}_3)} w_a w_b w_{c_0} w_{c_1} w_{c_2} w_{c_3} \cdot \begin{vmatrix} b & a & b \\ c_0 & c_0 & c_3 \end{vmatrix} \begin{vmatrix} b & a & b \\ c_1 & c_0 & c_0 \end{vmatrix} \\ \cdot \begin{vmatrix} b & a & b \\ c_1 & c_1 & c_0 \end{vmatrix} \begin{vmatrix} b & a & b \\ c_2 & c_1 & c_1 \end{vmatrix} \\ \cdot \begin{vmatrix} b & a & b \\ c_2 & c_2 & c_1 \end{vmatrix} \begin{vmatrix} b & a & b \\ c_3 & c_2 & c_2 \end{vmatrix} \\ \cdot \begin{vmatrix} b & a & b \\ c_3 & c_3 & c_2 \end{vmatrix} \begin{vmatrix} b & a & b \\ c_0 & c_3 & c_3 \end{vmatrix}.$$

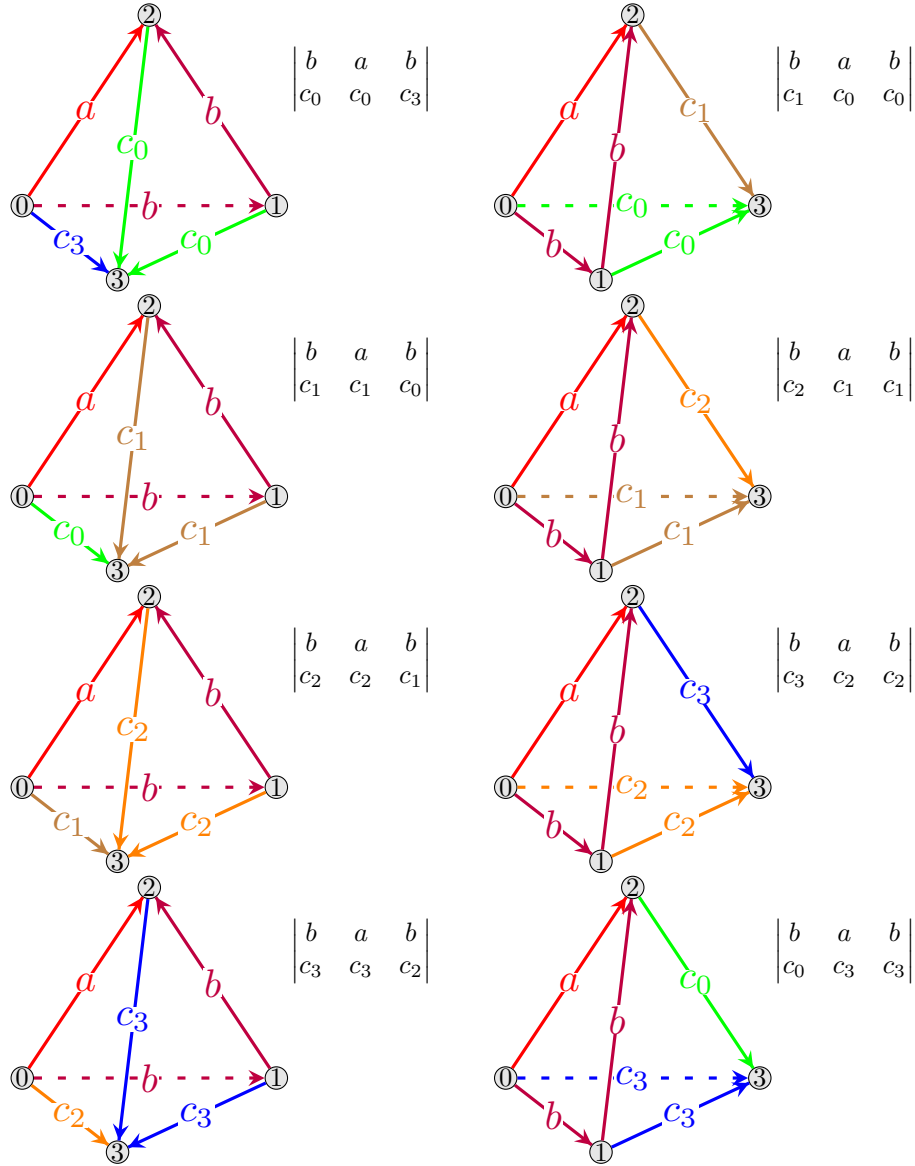


FIGURE 16. The coloring c of the ideal tetrahedra of \mathcal{T}_3 together with their respective tetrahedron terms

Using Proposition 3.6 and a bit of reordering, we can rewrite the summation as:

$$TV_{r,s}(M_3, \mathcal{T}_3) = \sum_{(a,b,c_0,c_1,c_2,c_3) \in \mathcal{A}_r(M_3, \mathcal{T}_3)} w_a w_b w_{c_0} w_{c_1} w_{c_2} w_{c_3} \cdot \begin{matrix} \begin{vmatrix} a & b & b \\ c_0 & c_0 & c_3 \end{vmatrix} \begin{vmatrix} a & b & b \\ c_0 & c_0 & c_1 \end{vmatrix} \\ \cdot \begin{vmatrix} a & b & b \\ c_1 & c_1 & c_0 \end{vmatrix} \begin{vmatrix} a & b & b \\ c_1 & c_1 & c_2 \end{vmatrix} \\ \cdot \begin{vmatrix} a & b & b \\ c_2 & c_2 & c_1 \end{vmatrix} \begin{vmatrix} a & b & b \\ c_2 & c_2 & c_3 \end{vmatrix} \\ \cdot \begin{vmatrix} a & b & b \\ c_3 & c_3 & c_2 \end{vmatrix} \begin{vmatrix} a & b & b \\ c_3 & c_3 & c_0 \end{vmatrix} \end{matrix}$$

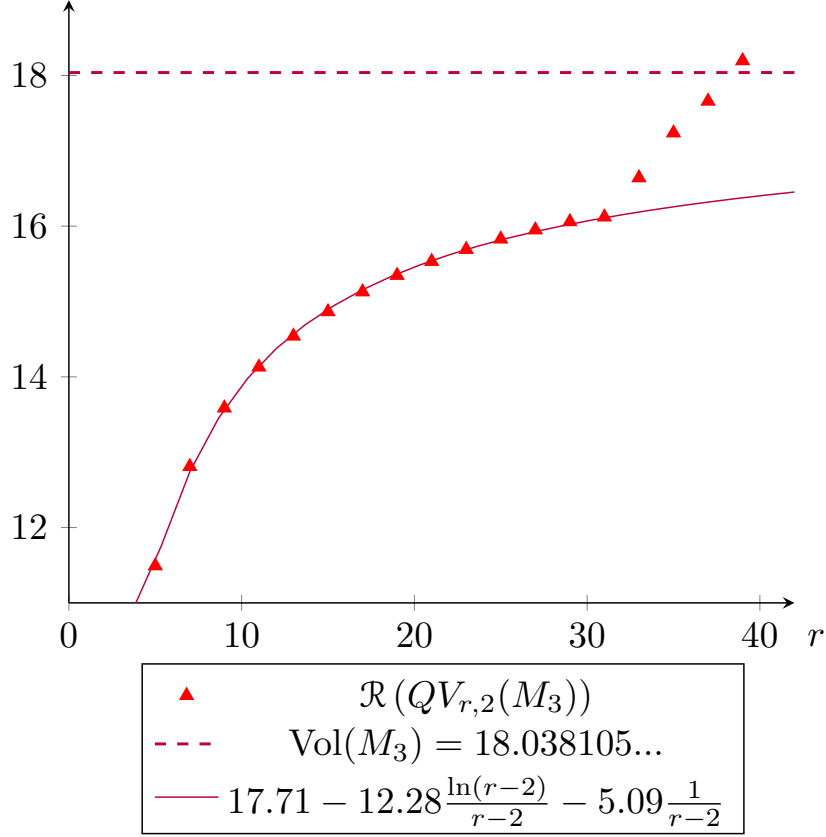


FIGURE 17. Graph of the values of $\mathcal{R}(QV_{r,2}(M_3))$ (for $5 \leq r \leq 39$, red triangles) compared with the hyperbolic volume $\text{Vol}(M_3)$ (red dashed line) and an interpolation of $\mathcal{R}(QV_{r,2}(M_3))$ for $r \leq 31$ (red curve).

6.2.4. *Numerical check of the volume conjecture.* Our conclusions and discussions are almost the same as for the example of M_2 in Section 6.1.4. The only differences are that the strange behavior starts appearing earlier, at $r = 31$ (which makes sense since there are more tetrahedra and thus more terms in the sums), and the constant term from the interpolating function is equal to the volume $\text{Vol}(M_3)$ up to 1.8%.

6.3. **The cases of M_4 to M_7 .** For $4 \leq g \leq 7$, we do not observe a strange behavior of $\mathcal{R}(QV_{r,2}(M_g))$ as r increases, and we can thus interpolate all available values with the model $a + b \cdot \frac{2\pi \ln(r-2)}{r-2} + c \frac{1}{r-2}$. The values of a, b, c are listed in Figure 11; all computed values of $\mathcal{R}(QV_{r,2}(M_g))$ and the associated interpolating functions are displayed in Figure 18.

We observe good fits to the model $a + b \cdot \frac{2\pi \ln(r-2)}{r-2} + c \frac{1}{r-2}$, with a equal to the expected hyperbolic volume $\text{Vol}(M_g)$ up to a few percents (see Figure 11). We conclude that the manifolds M_2, \dots, M_7 seem to satisfy Conjectures 1.1 and 1.2 numerically.

6.4. **Behavior of the coefficient $b(M_g)$ relative to g .** Let us now delve into Conjecture 1.3. In this section, we assume that Conjecture 1.2 holds for the manifolds M_2, \dots, M_7 (which is suggested numerically by the results of the previous sections). We then study whether or not the coefficient b grows linearly in g .

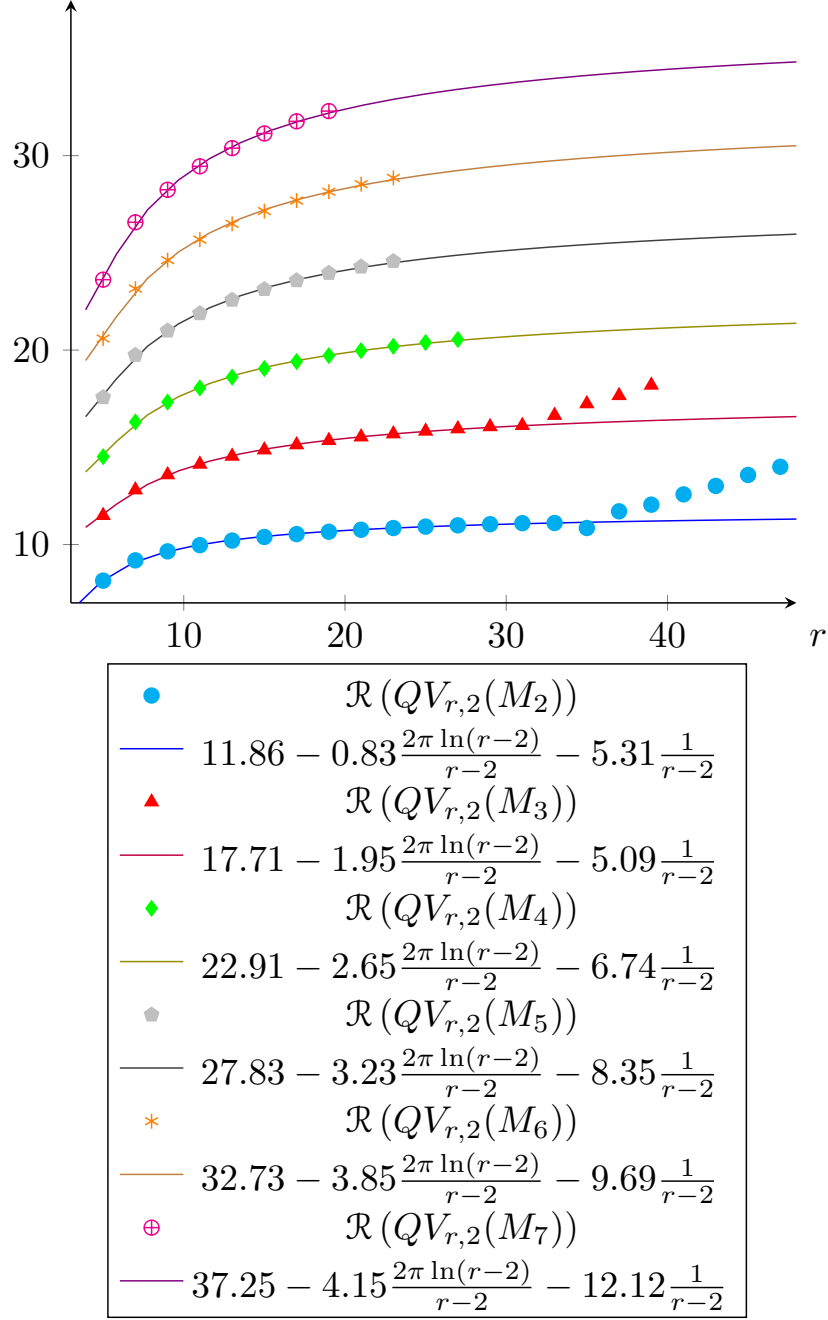


FIGURE 18. Graphs of the values of $\mathcal{R}(QV_{r,2}(M_g))$ in function of $r \geq 5$ (for $2 \leq g \leq 7$), compared with their respective best interpolations in the model $a + b \cdot \frac{2\pi \ln(r-2)}{r-2} + c \frac{1}{r-2}$.

Since we assume that Conjecture 1.2 holds for the manifolds M_2, \dots, M_7 , we can now fix $a = \text{Vol}(M_g)$ in the model $a + b \cdot \frac{2\pi \ln(r-2)}{r-2} + c \frac{1}{r-2}$, and look once again for the best interpolation.

Using `find_fit` with the new model $\text{Vol}(M_g) + b \cdot \frac{2\pi \ln(r-2)}{r-2} + c \frac{1}{r-2}$ yields different values for b, c than in Section 5.3. These new values are listed in Figure 19 and the corresponding interpolating functions are displayed in Figure 20.

g	r_{max}	$\text{Vol}(M_g)$	b	c
2	33	12.04609204	-1.07486449	-4.06269480
3	31	18.03810545	-2.36670389	-2.98774665
4	27	23.60349490	-3.47345292	-2.75451472
5	23	28.98945539	-4.50837608	-2.48549875
6	23	34.28064479	-5.55394983	-1.84727854
7	19	39.51512785	-6.43483298	-2.38715613

FIGURE 19. Values of the interpolating coefficients a, b, c for the model $\text{Vol}(M_g) + b \cdot \frac{2\pi \ln(r-2)}{r-2} + c \frac{1}{r-2}$ for $\mathcal{R}(QV_{r,2}(M_g))$, with $5 \leq r \leq r_{max}$.

As expected by their definitions, the interpolations of Figure 20 are less fitting than the ones of Figure 18, but they still seem satisfactory.

Figure 21 displays the values of the coefficient b in function of g (as black asterisks), with the corresponding best linear interpolation (the green line). The coefficient of determination of this linear interpolation is $R^2 = 0.9967$, which gives much credit to the hypothesis of the affine behaviour of b .

What precedes thus yields a satisfying numerical check of Conjecture 1.3 for the family of manifolds M_g .

More precisely, the interpolating affine function is computed to be

$$0.9061 - 1.068g.$$

Of course, more data would give us an interpolating affine function closer to the expected one, but as the slope -1.068 is already quite close to -1 , it is not unreasonable to look for a general behavior of b in the form of

$$b(M) \stackrel{?}{=} \text{constant} - \frac{1}{2}\chi(\partial M),$$

since in the specific case of Frigerio's manifolds we have

$$b(M_g) \underset{2 \leq g \leq 7}{\approx} \text{constant} - g = \text{constant} - \frac{1}{2}\chi(\partial M_g).$$

7. DISCUSSION AND FURTHER DIRECTIONS

- It would be interesting to understand the origin of the pattern breaks for $\mathcal{R}(QV_{r,2}(M_2))$ and $\mathcal{R}(QV_{r,2}(M_3))$. If, as we surmise, they come from numerical approximations by the machine for terms of different magnitudes, then this hypothesis could be tested by refining our code and examining the range of magnitudes of the terms in the sum when r grows larger. The works of Maria-Rouillé [12] seem like a promising direction to follow.
- Conjecture 1.3 appears to be satisfied for the manifolds M_g , but it would be interesting to test it for other families of manifolds with diverse boundary components. Furthermore, one could try to prove (or disprove!) rigorously that b has an affine behavior of the form $-\frac{1}{2}\chi(\partial M) + \text{constant}$, via combinatorial arguments on the triangulations (how the numbers of vertices, edges and tetrahedra are related to $\chi(\partial M)$) and asymptotics in r of the terms associated to regular vertices, edges and tetrahedra in the definition of the Turaev–Viro invariants.

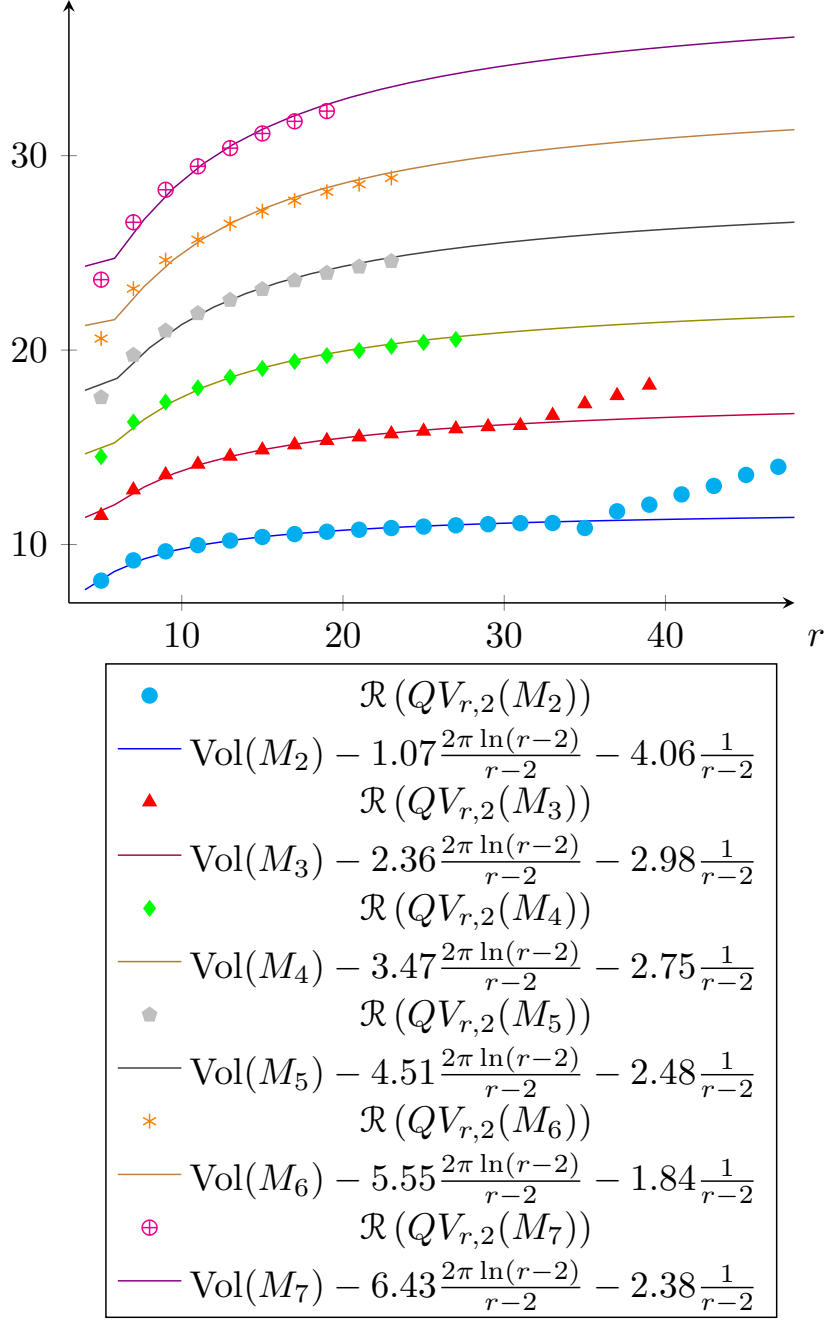


FIGURE 20. Graphs of the values of $\mathcal{R}(QV_{r,2}(M_g))$ in function of $r \geq 5$ (for $2 \leq g \leq 7$), compared with their respective best interpolations in the model $\text{Vol}(M_g) + b \cdot \frac{2\pi \ln(r-2)}{r-2} + c \frac{1}{r-2}$.

- The extended volume conjectures as stated in Conjectures 1.2 and 1.3 already (or may possibly) admit variants for other quantum invariants. Can the methods used in the present paper be applied for these other invariants? The manifolds M_g seem especially convenient to study for invariants defined on (ordered) triangulations.

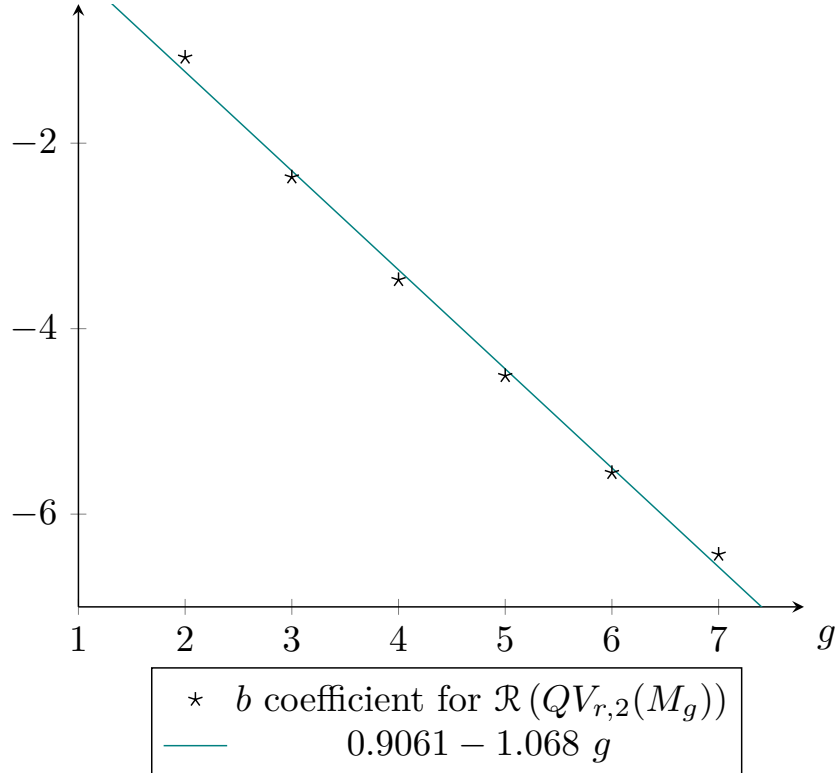


FIGURE 21. Values of the coefficient $b(M_g)$ for $2 \leq g \leq 7$ (black asterisks), and the associated interpolating affine function (green line), with coefficient of determination $R^2 = 0.9967$.

ACKNOWLEDGEMENTS

The first author was supported by the FNRS in his "Research Fellow" position at UCLouvain, under Grant no. 1B03320F. The second author would like to thank his two supervisors (Pedro Vaz and the first author) for their intellectual and emotional support throughout his Master's thesis that gave rise to the current paper. Both authors thank Pedro Vaz for his continuous involvement in the project, and Renaud Detcherry and François Costantino for helpful discussions.

REFERENCES

- [1] Fathi Ben Aribi, François Guéritaud and Eiichi Piguët-Nakazawa, *Geometric triangulations and the Teichmüller TQFT volume conjecture for twist knots*, 2020, [arXiv:1903.09480](https://arxiv.org/abs/1903.09480).
- [2] Qingtao Chen and Tian Yang, *A volume conjecture for a family of Turaev–Viro type invariants of 3-manifolds with boundary*, 2015, [arXiv:1503.02547v2](https://arxiv.org/abs/1503.02547).
- [3] Qingtao Chen and Tian Yang, *Volume conjectures for the Reshetikhin–Turaev and the Turaev–Viro invariants*, *Quantum Topol.*, 9(3):419–460, 2018.
- [4] Renaud Detcherry, Efstratia Kalfagianni and Tian Yang, *Turaev–Viro invariants, colored Jones polynomials, and volume*, *Quantum Topol.*, 9(4):775–813, 2018.
- [5] Roberto Frigerio, *An infinite family of hyperbolic graph complements in S^3* , *J. Knot Theory Ramifications*, 14(4):479–496, 2005.
- [6] Dongmin Gang, Mauricio Romo and Masahito Yamazaki, *All-Order Volume Conjecture for Closed 3-Manifolds from Complex Chern-Simons Theory*, 2017, [arXiv:1704.00918](https://arxiv.org/abs/1704.00918).
- [7] James Gosselet, *The Chen–Yang volume conjecture for knots in handlebodies*, *Faculté des sciences, UCLouvain*, 2021. Prom.: Ben Aribi, Fathi; Vaz, Pedro. Master's thesis.
- [8] Damian Heard, *Orb.Reference*, 2007, <https://github.com/DamianHeard/orb/blob/master/OrbDocumentation.pdf>.

- [9] Vaughan F. R. Jones, *A polynomial invariant for knots via von Neumann algebras*, Bull. Amer. Math. Soc. (N.S.), 12(1):103–111, 1985.
- [10] Rinat M. Kashaev, *The hyperbolic volume of knots from the quantum dilogarithm*, Lett. Math. Phys., 39(3):269–275, 1997.
- [11] Rinat M. Kashaev, Feng Luo and Grigory Vartanov, *A TQFT of Turaev–Viro type on shaped triangulations*, Ann. Henri Poincaré, 17(5):1109–1143, 2016.
- [12] Clément Maria and Owen Rouillé, *Computation of large asymptotics of 3-manifold quantum invariants*, Proceedings of SIAM Symposium on Algorithm Engineering and Experiments (ALENEX 2021), [arXiv:2010.14316](https://arxiv.org/abs/2010.14316).
- [13] Tomotada Ohtsuki, *On the asymptotic expansion of the quantum $SU(2)$ invariant at $q = \exp(4\pi\sqrt{-1}/N)$ for closed hyperbolic 3-manifolds obtained by integral surgery along the figure-eight knot*, Algebr. Geom. Topol., 18(7):4187–4274, 2018.
- [14] Jessica S. Purcell, *Hyperbolic knot theory*, volume 209 of Graduate Studies in Mathematics, American Mathematical Society, Providence, RI, [2020] © 2020.
- [15] Akira Ushijima, *A volume formula for generalised hyperbolic tetrahedra*, In Non-Euclidean geometries, volume 581 of Math. Appl. (N. Y.), pages 249–265. Springer, New York, 2006.
- [16] Ka Ho Wong, *Asymptotics of some quantum invariants of the Whitehead chains*, 2019, [arXiv:1912.10638](https://arxiv.org/abs/1912.10638).

UCLouvain, IRMP, CHEMIN DU CYCLOTRON 2, 1348 LOUVAIN-LA-NEUVE, BELGIUM
Email address: fathi.benaribi@uclouvain.be

UCLouvain, IRMP, CHEMIN DU CYCLOTRON 2, 1348 LOUVAIN-LA-NEUVE, BELGIUM
Email address: james.gosselet@student.uclouvain.be